

Fully-discrete provably Lyapunov consistent discretizations for convection-diffusion-reaction PDE systems

Rasha Al Jahdali^{1,*}, David C. Del Rey Fernández², Lisandro Dalcin¹,
Matteo Parsani^{1,3}

¹Computer Electrical and Mathematical Science and Engineering Division (CEMSE),
King Abdullah University of Science and Technology (KAUST), Thuwal, 23955-6900,
Saudi Arabia.

² Department of Applied Mathematics, University of Waterloo, Waterloo, Canada.

³Physical Science and Engineering Division (PSE), King Abdullah University of Science
and Technology (KAUST), Thuwal, 23955-6900, Saudi Arabia.

*Corresponding author(s). E-mail(s): rasha.aljahdali@kaust.edu.sa;

Contributing authors: ddelreyfernandez@uwaterloo.ca; dalcinl@gmail.com;
matteo.parsani@kaust.edu.sa;

Abstract

Convection-diffusion-reaction equations are a class of second-order partial differential equations widely used to model phenomena involving the change of concentration/population of one or more substances/species distributed in space. Understanding and preserving their stability properties in numerical simulation is crucial for accurate predictions, system analysis, and decision-making. This work presents a comprehensive framework for constructing fully discrete Lyapunov-consistent discretizations of any order for convection-diffusion-reaction models. We introduce a systematic methodology for constructing discretizations that mimic the stability analysis of the continuous model using Lyapunov's direct method. The spatial algorithms are based on collocated discontinuous Galerkin methods with the summation-by-parts property and the simultaneous approximation terms approach for imposing interface coupling and boundary conditions. Relaxation Runge-Kutta schemes are used to integrate in time and achieve fully discrete Lyapunov consistency. To verify the properties of the new schemes, we numerically solve a system of convection-diffusion-reaction partial differential equations governing the dynamic evolution of monomer and dimer concentrations during the dimerization process. Numerical results demonstrated the accuracy and consistency of the proposed discretizations. The new framework can enable further advancements in the analysis, control, and understanding of general convection-diffusion-reaction systems.

Keywords: Convection-diffusion-reaction equations, Lyapunov functionals, Summation-by-parts operators, Relaxation Runge-Kutta schemes, Fully-discrete Lyapunov-consistent discretizations.

1 Introduction

Convection-diffusion-reaction partial differential equations (PDEs) are a class of time-dependent second-order PDEs that can describe the dynamics of substance concentrations in a medium under the influence of convection, diffusion, and reaction processes. These PDEs are often used to describe different phenomena, including fluid dynamics, plasma physics, biological population genetics, neurology, heat transfer, combustion, and reaction chemistry.

Stability analysis is fundamental to understanding the dynamics governing convection-diffusion-reaction models (e.g., stability of equilibrium points and input-output stability). Lyapunov’s second method, also known as Lyapunov’s direct method, is a rigorous approach to analyzing the asymptotic behavior and stability of dynamical systems modeled using ordinary differential equations (ODEs). This approach uses a generalized notion of energy functions (i.e., Lyapunov functions) to address stability.

Lyapunov’s direct method has been successfully used in the PDE context to, for example, study the stability of fixed points and the stabilization of distributed parameter PDEs [1–7]. In the PDEs context, the conventional Lyapunov function is replaced by a Lyapunov functional which is typically constructed by integrating an appropriate Lyapunov function over the spatial domain. However, generating Lyapunov functionals is nontrivial. Nevertheless, many studies have made significant progress in identifying and constructing Lyapunov functionals for specific classes of PDEs, thereby contributing to understanding stability properties and enabling further advancements in control and system analysis.

Recently, Al Jahdali and collaborators [8] have developed discretizations for (parabolic) reaction-diffusion PDEs that mimic the Lyapunov stability properties of the continuous models. The construction of those discretizations is rooted in Lyapunov’s direct method. Hence, they are referred to as “Lyapunov consistent” discretizations. In this work, starting from the framework presented in [8], we develop fully discrete Lyapunov consistent discretizations that preserve the stability properties of continuous convection-reaction-diffusion PDE models. To design Lyapunov consistent schemes for this class of PDEs, the analysis of the convective term requires additional considerations. Here, we develop appropriate two-point flux functions [9] that render convective terms and result in Lyapunov consistent algorithms.

In this work, we present a general framework that enables the construction of fully discrete Lyapunov consistent discretizations that are high-order in space and time. The algorithms are devised to ensure provable stability, emulating the continuous stability proofs used in Lyapunov’s direct method. In the stability analysis of PDE models, integration by parts (IBP) often plays a vital role. Thus, it is natural to leverage a class of spatial operators that discretely mimic IBP. Within this class, known as the summation-by-parts (SBP) methods [10, 11], the discrete analog of IBP serves as a fundamental design principle. At the spatial level, the proposed methods are constructed using the SBP approach. Specifically, the one-dimensional baseline spatial discretizations are collocated discontinuous Galerkin (DG) methods with the SBP property built at the Legendre–Gauss–Lobatto (LGL) quadrature points [12, 13]. The DG-SBP operators are then extended to multiple dimensions through tensor products. The semi-discrete Lyapunov consistency across the computational domain is achieved by combining the SBP operators with the simultaneous approximation terms (SAT) approach for the inter-element coupling and the enforcement of boundary conditions. The SAT methodology was originally developed in the context of linear stability [14–17] and subsequently extended to address nonlinear (entropy) stability [18, 19]. Additionally, the methodology described in [19] is used to apply these DG-SBP-SAT discretizations to curvilinear grids with geometric (h) and polynomial (p) refinements. To ensure fully discrete Lyapunov consistency and avoid spurious numerical solutions, the time integration procedure is performed using relaxation Runge–Kutta (RK) schemes [20, 21]. These temporal integration techniques can incorporate properties such as conservation, dissipation, or other solution properties associated with convex functionals, such as Lyapunov functionals. This remarkable feature is accomplished by multiplying the Runge–Kutta update at each time step by a relaxation parameter.

To demonstrate the properties of the new numerical framework, we solve a system of convection-diffusion-reaction PDEs that describe the dynamic evolution of monomer and dimer concentrations during the dimerization process. The algorithms are implemented in the high-performance computing SSDC framework [22], specifically designed and optimized to exploit spatial and temporal discretization properties and address the scalability and robustness requirements for complex simulations.

The paper is organized as follows. In Section 2, in the framework of Lyapunov’s direct method, we introduce and discuss the concept of “Lyapunov consistency.” Section 3 briefly discusses that the PDE extensions of ODE models inherit the ODE model’s equilibrium points. In Section 4, the spatial discretization framework for developing Lyapunov consistent collocated discontinuous Galerkin schemes with the summation-by-part property is presented. Section 5 summarizes the results of the relaxation Runge–Kutta schemes, which allow the design of fully discrete Lyapunov consistent algorithms. In Section 6, extensive numerical results, including convergence studies, are presented to demonstrate the accuracy and stability properties of the proposed algorithms. Finally, conclusions are drawn in Section 7.

2 Lyapunov Consistency

In this work, we consider a system of nonlinear convection-diffusion-reaction equations in dim spatial dimensions having r species. This system of PDEs written in conservation (or divergence) form reads

$$\frac{\partial \mathbf{U}}{\partial t} = \mathbf{R} - \sum_{l=1}^{dim} \frac{\partial \mathbf{F}_{x_l}^{(c)}}{\partial x_l} + \sum_{l=1}^{dim} \frac{\partial \mathbf{F}_{x_l}^{(d)}}{\partial x_l}, \quad \mathbf{x} \in \Omega, \quad t \in (t_0, T_f], \quad (1)$$

where $\mathbf{U} \in \mathbb{R}^r$, $\mathbf{R} = \mathbf{R}(\mathbf{U})$ contains the reaction terms, and $\mathbf{F}_{x_l}^{(c)} = \mathbf{F}_{x_l}^{(c)}(\mathbf{U}) \in \mathbb{R}^{r \times dim}$ and $\mathbf{F}_{x_l}^{(d)} = \mathbf{F}_{x_l}^{(d)}\left(\mathbf{U}, \frac{\partial \mathbf{U}}{\partial x_l}\right) \in \mathbb{R}^{r \times dim}$ are the convective and diffusive fluxes in the l^{th} coordinate direction, respectively. The position vector is defined as $\mathbf{x} = (x_1, \dots, x_{dim})^T \in \Omega$, where $\Omega \in \mathbb{R}^{dim}$ is the spatial domain with boundary Γ . The symbol T_f indicates the final time, i.e., the upper bound of the time interval. The viscous flux components in (1) are defined as

$$\mathbf{F}_{x_l}^{(d)} = \mathbf{C}_{l,m} \frac{\partial \mathbf{U}}{\partial x_m}, \quad (2)$$

where $\mathbf{C}_{l,m}$ is the $r \times r$ matrix of the diffusion coefficients for the conservative variable, \mathbf{U} . Finally, because system (1) corresponds to an initial boundary value problem, we have to close it with an initial condition, $\mathbf{U}(\mathbf{x}, t_0) = \mathbf{U}^0$, and appropriate boundary conditions.

In what follows, we derive the time rate of change of the Lyapunov functional, \tilde{V} , which represents a generalized energy function for system (1) when it can be constructed. As shown later in the section, the time derivative of \tilde{V} can be used in conjunction with LaSalle's invariance principle [23, 24] to investigate the stability of the fixed points of several PDE models, which can be rewritten as (1). Many of the steps used in the procedure described next follow the landmark works of Harten [25] and Tadmor [9, 26] for systems of conservation laws. These steps also resemble those used in the entropy analysis of the compressible Euler and Navier–Stokes equations. It is important to highlight that the advancement of mathematical theory for nonlinear conservation law systems has been documented over the years in various monographs and books. This journey began with the seminal work of Courant and Hilbert in 1962 [27], followed by contributions from Lax in 1973 [28], Smoller in 1983 [29], Whitham in 1999 [30], Serre in 2000 [31], Bressan in 2000 [32], and Dafermos in 2016 [33].

We begin by assuming that a convex Lyapunov function [34], $V = V(\mathbf{U})$, for system (1) exists and can be explicitly generated. The convexity of the Lyapunov function means that its Hessian is positive definite, i.e.,

$$\zeta^T \frac{\partial^2 V}{\partial \mathbf{U}^2} \zeta > 0, \quad \text{for all nonzero vectors } \zeta. \quad (3)$$

Often, the Lyapunov functional, \tilde{V} , is constructed as

$$\tilde{V} \equiv \int_{\Omega} V d\Omega. \quad (4)$$

Next, we define the Lyapunov variables (i.e., the entropy variables in [25, 26]) as

$$\mathbf{W} \equiv \left(\frac{\partial V}{\partial \mathbf{U}} \right)^T, \quad (5)$$

where the convexity of V ensures that there is a one-to-one correspondence between the (state) conservative variables, \mathbf{U} , and the Lyapunov variables, \mathbf{W} . Because of the one-to-one mapping, the variables \mathbf{U} can be written as a function of the Lyapunov variables, i.e., $\mathbf{U} = \mathbf{U}(\mathbf{W})$.

At this point, it is useful to recast the diffusion contribution in system (1), $\mathbf{F}_{x_l}^{(d)}$, in terms of the Lyapunov variables, i.e.,

$$\mathbf{F}_{x_l}^{(d)} = \hat{\mathbf{C}}_{l,m} \frac{\partial \mathbf{W}}{\partial x_m}, \quad (6)$$

where $\widehat{\mathbf{C}}_{l,m} \equiv \mathbf{C}_{l,m} \frac{\partial \mathbf{U}}{\partial \mathbf{W}}$ is the $r \times r$ matrix of the diffusion coefficients in the new set of variables, \mathbf{W} . Thus, system (1) can be rewritten as

$$\frac{\partial \mathbf{U}}{\partial t} = \mathbf{R} - \sum_{l=1}^{dim} \frac{\partial \mathbf{F}_{x_l}^{(c)}}{\partial x_l} + \sum_{l,m=1}^{dim} \frac{\partial}{\partial x_l} \left(\widehat{\mathbf{C}}_{l,m} \frac{\partial \mathbf{W}}{\partial x_m} \right). \quad (7)$$

Furthermore, we assume that the following matrix:

$$\widehat{\mathbf{M}} \equiv \begin{bmatrix} \widehat{\mathbf{C}}_{1,1} & \dots & \widehat{\mathbf{C}}_{1,dim} \\ \vdots & & \vdots \\ \widehat{\mathbf{C}}_{dim,1} & \dots & \widehat{\mathbf{C}}_{dim,dim} \end{bmatrix} \quad (8)$$

is such that $\widehat{\mathbf{M}} + \widehat{\mathbf{M}}^T$ is positive semi-definite, i.e., $\widehat{\mathbf{M}} + \widehat{\mathbf{M}}^T \geq 0$.

Remark 1. *The assumption that $\widehat{\mathbf{M}} + \widehat{\mathbf{M}}^T \geq 0$ is the major assumption in this paper and allows us to completely decouple the analysis of the diffusion from that of the convection and reaction terms.*

To obtain the time derivative of the Lyapunov functional, $d\tilde{V}/dt$, we proceed as follows. We multiply from the left Equation (7) by \mathbf{W}^T , which results in

$$\mathbf{W}^T \frac{\partial \mathbf{U}}{\partial t} = \mathbf{W}^T \mathbf{R} - \sum_{l=1}^{dim} \mathbf{W}^T \frac{\partial \mathbf{F}_{x_l}^{(c)}}{\partial x_l} + \sum_{l,m=1}^{dim} \mathbf{W}^T \frac{\partial}{\partial x_l} \left(\widehat{\mathbf{C}}_{l,m} \frac{\partial \mathbf{W}}{\partial x_m} \right). \quad (9)$$

Then, we integrate over the domain Ω :

$$\int_{\Omega} \mathbf{W}^T \frac{\partial \mathbf{U}}{\partial t} d\Omega = \int_{\Omega} \mathbf{W}^T \mathbf{R} d\Omega - \int_{\Omega} \sum_{l=1}^{dim} \mathbf{W}^T \frac{\partial \mathbf{F}_{x_l}^{(c)}}{\partial x_l} d\Omega + \int_{\Omega} \sum_{l,m=1}^{dim} \mathbf{W}^T \frac{\partial}{\partial x_l} \left(\widehat{\mathbf{C}}_{l,m} \frac{\partial \mathbf{W}}{\partial x_m} \right) d\Omega. \quad (10)$$

The temporal term reduces as follows:

$$\int_{\Omega} \mathbf{W}^T \frac{\partial \mathbf{U}}{\partial t} d\Omega = \int_{\Omega} \frac{\partial V}{\partial \mathbf{U}} \frac{\partial \mathbf{U}}{\partial t} d\Omega = \int_{\Omega} \frac{\partial V}{\partial t} d\Omega = \frac{d}{dt} \int_{\Omega} V d\Omega, \quad (11)$$

where in the last step we used the Leibniz's rule. The viscous terms is rewritten using the multidimensional IBP rule as follows:

$$\begin{aligned} \int_{\Omega} \sum_{l,m=1}^{dim} \mathbf{W}^T \frac{\partial}{\partial x_l} \left(\widehat{\mathbf{C}}_{l,m} \frac{\partial \mathbf{W}}{\partial x_m} \right) d\Omega &= \oint_{\Gamma} \sum_{l,m=1}^{dim} \mathbf{W}^T \widehat{\mathbf{C}}_{l,m} \frac{\partial \mathbf{W}}{\partial x_m} n_{x_l} d\Gamma - \int_{\Omega} \sum_{l,m=1}^{dim} \frac{\partial \mathbf{W}^T}{\partial x_l} \widehat{\mathbf{C}}_{l,m} \frac{\partial \mathbf{W}}{\partial x_m} d\Omega \\ &= \oint_{\Gamma} \sum_{l,m=1}^{dim} \mathbf{W}^T \widehat{\mathbf{C}}_{l,m} \frac{\partial \mathbf{W}}{\partial x_m} n_{x_l} d\Gamma - \int_{\Omega} \mathbf{Z}^T \widehat{\mathbf{M}} \mathbf{Z} d\Omega, \end{aligned} \quad (12)$$

where n_{x_l} is the component of the outward facing normal on the boundary Γ in the direction x_l , $\mathbf{Z} \equiv [\partial \mathbf{W} / \partial x_1, \dots, \partial \mathbf{W} / \partial x_{dim}]^T$, and $\widehat{\mathbf{M}}$ is the matrix defined in Equation (8). Note that one could obtain expression (12) by using the product rule first and then the divergence theorem [8]. The convective

contribution is manipulated as follows:

$$\begin{aligned}
\int_{\Omega} \sum_{l=1}^{dim} \mathbf{W}^T \frac{\partial \mathbf{F}_{x_l}^{(c)}}{\partial x_l} d\Omega &= \int_{\Omega} \sum_{l=1}^{dim} \frac{\partial V}{\partial \mathbf{U}} \frac{\partial \mathbf{F}_{x_l}^{(c)}}{\partial \mathbf{U}} \frac{\partial \mathbf{U}}{\partial x_l} d\Omega, \\
&= \int_{\Omega} \sum_{l=1}^{dim} \frac{\partial \mathfrak{F}_{x_l}}{\partial \mathbf{U}} \frac{\partial \mathbf{U}}{\partial x_l} d\Omega, \\
&= \int_{\Omega} \sum_{l=1}^{dim} \frac{\partial \mathfrak{F}_{x_l}}{\partial x_l} d\Omega, \\
&= \oint_{\Gamma} \sum_{l=1}^{dim} \mathfrak{F}_{x_l} n_{x_l} d\Gamma,
\end{aligned} \tag{13}$$

with

$$\frac{\partial V}{\partial \mathbf{U}} \frac{\partial \mathbf{F}_{x_l}^{(c)}}{\partial \mathbf{U}} = \frac{\partial \mathfrak{F}_{x_l}}{\partial \mathbf{U}}, \tag{14}$$

where the scalar function $\mathfrak{F}_{x_l} = \mathfrak{F}_{x_l}(\mathbf{U})$ is the Lyapunov flux (i.e., the entropy flux in [9, 25]) in the x_l coordinate direction, corresponding to the Lyapunov function $V = V(\mathbf{U})$. The last expression in (13) shows that the contribution of convective terms to the time rate of change of the Lyapunov functional is “only” a boundary term. This feature/property is often referred to as the “telescoping” property; see [35] where this terminology was introduced in the context of fluid dynamics.

Using Equations (11)-(13), expression (10) becomes

$$\frac{d\tilde{V}}{dt} = \frac{d}{dt} \int_{\Omega} V d\Omega = \int_{\Omega} \mathbf{W}^T \mathbf{R} d\Omega + \oint_{\Gamma} \left(- \sum_{l=1}^{dim} \mathfrak{F}_{x_l} + \sum_{l,m=1}^{dim} \mathbf{W}^T \hat{\mathbf{C}}_{l,m} \frac{\partial \mathbf{W}}{\partial x_m} \right) n_{x_l} d\Gamma - \int_{\Omega} \mathbf{Z}^T \hat{\mathbf{M}} \mathbf{Z} d\Omega. \tag{15}$$

Equation (15) provides the expression of the time rate of change of the Lyapunov functional, \tilde{V} , for the PDE model (1).

Lyapunov’s direct method, when combined with LaSalle’s invariance principle, can be used to analyze the stability of infinite dimensional systems, such as PDE systems, under the following conditions: i) a Lyapunov functional, \tilde{V} , exists and can be generated for the dynamical system of interest, and ii) the trajectories of the dynamical system are contained within a compact set [36, 37]. When these two conditions are satisfied, the following result holds:

Theorem 1. *Consider the existence of the equilibrium point \mathbf{U}_{eq} of system (7), (i.e., a point in phase space such that the right-hand side of system (7) is zero) where each of its components is bounded. Furthermore, assume that the following conditions are met:*

1. V is convex and locally positive definite,
2. $\mathbf{W}^T \mathbf{R} \leq 0$,
3. $\hat{\mathbf{M}} + \hat{\mathbf{M}}^T \geq 0$,
4. Appropriate boundary conditions can be found such that

$$\oint_{\Gamma} \left(- \sum_{l=1}^{dim} \mathfrak{F}_{x_l} + \sum_{l,m=1}^{dim} \mathbf{W}^T \hat{\mathbf{C}}_{l,m} \frac{\partial \mathbf{W}}{\partial x_m} \right) n_{x_l} d\Gamma \leq 0.$$

Then, defining the Lyapunov functional

$$\tilde{V} \equiv \int_{\Omega} V d\Omega, \tag{16}$$

we have the following stability result:

- If \tilde{V} is locally positive definite, $d\tilde{V}/dt$ is negative definite, and $\|\mathbf{U}\| \rightarrow +\infty \Rightarrow \tilde{V}(\mathbf{U}) \rightarrow +\infty$, then $\mathbf{U}_{eq} = 0$ is globally asymptotically stable.

Proof. Under the stated conditions equation (15) reduces to

$$\frac{d\tilde{V}}{dt} \leq 0.$$

The Lyapunov functional, \tilde{V} , is locally positive since V is locally positive and $\frac{d\tilde{V}}{dt} = 0$ at the equilibrium point, \mathbf{U}_{eq} . Thus, the Lyapunov function, V , can be converted into a Lyapunov functional, \tilde{V} , with the same properties. Then, we apply the LaSalle's invariance principle to prove the stability statement for the fix point \mathbf{U}_{eq} . \square

In this work, we develop a systematic framework to design fully discrete algorithms for system (7), which mimic at the discrete level the properties of the Lyapunov functional, \tilde{V} , and its time derivative, $d\tilde{V}/dt$, listed in Theorem 1. These algorithms are referred to as Lyapunov-consistent discretizations and mimic term-by-term each contribution appearing in equation (15).

3 From ODEs to PDEs: Equilibrium points

In some modeling approaches, spatially varying models are built from ODE models and a natural questions that arises is if the PDE extension inherits the equilibrium points of the ODE model. In the context of convection-diffusion-reaction models considered here, we have the following theorem:

Theorem 2. *If the convection-diffusion-reaction model (1) is the PDE extension of the ODE model*

$$\frac{d\mathbf{U}}{dt} = \mathbf{R}(\mathbf{U}) \quad t \in (t_0, T_f],$$

then, it inherits the equilibrium points of the ODE model.

Proof. Since the inherited equilibrium points in the PDE context are constant in space, the spatial terms in Equation (1) are zero. Since \mathbf{R} must also be zero at an equilibrium point of the ODE model, we see that the ODE's equilibrium points must be the PDE's equilibrium points. \square

4 Spatial discretization: diffusion and convection

In this section, we present our spatial discretization framework. The goal is to develop schemes that are Lyapunov consistent, i.e., they mimic term-by-term each contribution appearing in Equation (15) which governs at the continuous level the evolution of the spatial integral of the Lyapunov function. To construct such schemes, we rely on the SBP framework [10, 11, 38, 39] to derive discrete operators which approximate derivatives and SATs to enforce inter-element coupling and boundary conditions weakly [14, 16, 17, 40–46]. SBP operators are built to discretely mimic the IBP rule, while SATs are used to extend this property over the entire mesh, including the imposition of boundary conditions. SBP operators are typically constructed in a fixed computational domain and construct approximations to Cartesian derivatives over an element. Here, to simplify the presentation of the semi-discretization of (7) and the ensuing stability analysis, we use the resultant global SBP operators from the procedure mentioned above. Their construction is detailed in Appendix A. We refer the reader to [47] for a discussion on global SBP operators, and [48, 49] for a related discussion on constructing Cartesian SBP operators from computational SBP operators. While the global SBP perspective is helpful for presentation and analysis, implementing these schemes is generally done using the local element description. We provide details on the curvilinear element-wise discretization in Appendix B.

4.1 Preliminaries

When solving PDEs numerically, the physical domain Ω with boundary Γ , characterized by Cartesian coordinates (e.g., in three dimensions, $\mathbf{x} = (x_1, x_2, x_3) \in \mathbb{R}^3$) is partitioned into a set of K non-overlapping elements. The domain of the element with index κ is denoted by Ω^κ , and its boundary is denoted by Γ^κ . Thus, $\Omega = \bigcup_{\kappa=1}^K \Omega^\kappa$. We assume that Ω^κ is piecewise smooth for all elements κ . Without loss of generality, this work considers a partition (or tessellation) of the domain Ω accomplished

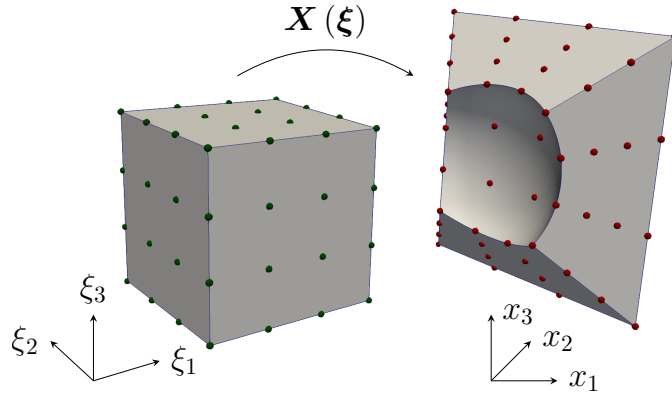


Fig. 1: The reference element and its mapping to an element in a 3D mesh.

with tensor-product elements, i.e., quadrilateral in two dimensions (2D) or hexahedral elements in three dimensions (3D). Numerically, we solve PDEs in computational coordinates $\boldsymbol{\xi} = (\xi_1, \xi_2, \xi_3)^T \in \mathbb{R}^3$, where each Ω^κ is logically transformed to the reference element $\hat{\Omega}^\kappa$, with boundary $\hat{\Gamma}^\kappa$, using a pull-back curvilinear coordinate transformation which satisfies the following assumption:

Assumption 1. *Each element in physical space is transformed using a local and invertible curvilinear coordinate transformation that is compatible at shared interfaces, meaning that the push-forward element-wise mappings are continuous across physical element interfaces. Note that this is the standard assumption requiring that the curvilinear coordinate transformation is water-tight.*

Precisely, one maps from the reference coordinates $\boldsymbol{\xi} \in [-1, 1]^{dim}$ to the physical element (see Figure 1 for the 3D case) by the push-forward transformation

$$\boldsymbol{x} = X(\boldsymbol{\xi}), \quad (17)$$

which, in the presence of curved elements, is usually a high-order degree polynomial. In our algorithm, we use a cell-wise isoparametric approach based on Lagrange basis functions. However, any set of polynomial basis functions and corresponding dual coefficients could be used to characterize the push-forward mapping (17). As usual in unstructured mesh schemes, the procedure described in what follows does not require explicit knowledge nor construction of the pull-back mappings.

Since derivatives are approximated with differentiation operators defined in computational space, we use the Jacobian of the push-forward mapping and the chain rule

$$\frac{\partial}{\partial x_l} = \sum_{m=1}^{dim} \frac{\partial \xi_m}{\partial x_l} \frac{\partial}{\partial \xi_m}, \quad \frac{\partial^2}{\partial x_l^2} = \sum_{m,a=1}^{dim} \frac{\partial \xi_m}{\partial x_l} \frac{\partial}{\partial \xi_m} \left(\frac{\partial \xi_a}{\partial x_l} \frac{\partial}{\partial \xi_a} \right),$$

to transform the PDEs from physical, \boldsymbol{x} , to computational space, $\boldsymbol{\xi}$. From here onward, we denote the determinant of the metric Jacobian by the symbol J .

Herein, we discretize functions using their nodal values. Suppose we have a set of N nodes placed in the domain Ω whose coordinates are stored in $\boldsymbol{x}^g = \{(x_{i,1}, \dots, x_{i,dim})\}_{i=1}^N$. Then, a generic continuous function $U \in L^2(\Omega)$ evaluated at the nodes is represented using the column vector

$$\boldsymbol{u}^g = (U(x_{1,1}, \dots, x_{1,dim}), U(x_{2,1}, \dots, x_{2,dim}), \dots, U(x_{N,1}, \dots, x_{N,dim})) \in \mathbb{R}^{rN}.$$

Note that the superscript “ g ” in \boldsymbol{x}^g and \boldsymbol{u}^g stands for “global”. This superscript is used for all the quantities that span the domain Ω , as opposed to the local quantities and operators associated with each element κ with volume Ω^κ . We can now present the global SBP operators for the first derivative and their properties. The details of each component of these operators are presented in Appendix A.

Definition 1. Consider a domain Ω partitioned by K non-overlapping elements resulting in a tessellation of the boundary surface Γ with M surfaces, where each face belongs to a uniquely defined element. Then, the order p global, diagonal norm, skew-symmetric SBP operator $\mathbf{D}_{x_i}^{s,g} \in \mathbb{R}^{(N \times r) \times (N \times r)}$ approximating the first derivative $\partial/\partial x_i$ for a system of r equations (i.e., $\partial \mathbf{U}/\partial x_i$, $\mathbf{U} \in \mathbb{R}^r$) on the N node nodal distribution \mathbf{x}^g has the following properties.

1. $\mathbf{D}_{x_i}^{s,g} \mathbf{u}^g \approx \frac{\partial \mathbf{U}}{\partial x_i}(\mathbf{x}^g) + \mathcal{O}(\Delta x^p)$,
2. $\mathbf{D}_{x_i}^{s,g} \equiv (\mathbf{P}_J^g)^{-1} \mathbf{Q}_{x_i}^{s,g}$, where the norm matrix, $\mathbf{P}_J^g = \mathbf{P}^g[J]$, is diagonal and positive definite,
3. $\mathbf{Q}_{x_i}^{s,g} \equiv \mathbf{S}_{x_i}^{s,g} + \frac{1}{2} \mathbf{E}_{x_i}^g$, where $\mathbf{S}_{x_i}^{s,g} = -(\mathbf{S}_{x_i}^{s,g})^\top$, $\mathbf{E}_{x_i}^g = (\mathbf{E}_{x_i}^g)^\top$,
4. the matrix $\mathbf{E}_{x_i}^g$ is diagonal and is constructed as,

$$\mathbf{E}_{x_i}^g \equiv \sum_{i=1}^M n_{\xi_{\Gamma_i}} (\mathbf{R}_{\xi_{\Gamma_i}})^\top \mathbf{P}_{\xi_{\Gamma_i}}^\perp \mathbf{R}_{\xi_{\Gamma_i}} \left[J \frac{\partial \xi_{\Gamma_i}}{\partial x_m} \right], \quad (18)$$

where Γ_i specifies the computational coordinate orthogonal to the i^{th} surface (i.e., in three dimensions Γ_i can assume the value 1 or 2 or 3). The diagonal matrices $\left[J \frac{\partial \xi_i}{\partial x_i} \right]_i$ contain the metric terms along their diagonal. Furthermore, the action of the matrices $\mathbf{R}_{\xi_{\Gamma_i}}$ is to pick off the appropriate portions of the solution vector at the i^{th} boundary surface which belongs to Γ . Thus, $\mathbf{R}_{\xi_{\Gamma_i}} \mathbf{u}^g$ results in a vector whose entries are the portion of the global solution vector \mathbf{u}^g at the boundary surface with index i , which belongs to Γ .

The diagonal matrices $\mathbf{P}_{\xi_{\Gamma_i}}^\perp$ contain cubature weights for the same i^{th} surface. The diagonal matrix $[J]$ used to construct \mathbf{P}_J^g is a diagonal matrix with the metric Jacobian, J , of each node along its diagonal.

The matrices that appear in Definition 1 are closely related to integral bilinear forms; see [50] for the case of multidimensional SBP operators. For completeness, we report their relationships. The diagonal matrix \mathbf{P}_J^g can be interpreted as a lumped mass matrix and can be used to approximate an inner product of two functions, e.g., their L^2 inner product. For instance, given two column vectors $\mathbf{U}, \mathbf{V} \in \mathbb{R}^r$ whose r components, U_i, V_i , are given by square integrable functions over the domain Ω (i.e., $U_i = U_i(\mathbf{x}), V_i = V_i(\mathbf{x}) \in L^2(\Omega)$, $i = 1, \dots, r$) we have:

$$(\mathbf{v}^g)^\top \mathbf{P}_J^g \mathbf{u}^g \approx \int_{\Omega} \mathbf{V}^\top \mathbf{U} \, d\Omega. \quad (19)$$

Furthermore, for the matrix $\mathbf{Q}_{x_i}^{s,g}$ we have that

$$(\mathbf{v}^g)^\top \mathbf{Q}_{x_i}^{s,g} \mathbf{u}^g \approx \int_{\Omega} \mathbf{V}^\top \frac{\partial \mathbf{U}}{\partial x_i} \, d\Omega \quad (20)$$

and

$$(\mathbf{v}^g)^\top (\mathbf{Q}_{x_i}^{s,g})^\top \mathbf{u}^g \approx \int_{\Omega} \left(\frac{\partial \mathbf{V}}{\partial x_i} \right)^\top \mathbf{U} \, d\Omega. \quad (21)$$

Finally, we note that the matrix $\mathbf{E}_{x_i}^g$ can be interpreted as an approximation the the following surface integral:

$$(\mathbf{v}^g)^\top \mathbf{E}_{x_i}^g \mathbf{u}^g \approx \oint_{\Gamma} \mathbf{V}^\top \mathbf{U} n_{x_i} \, d\Gamma. \quad (22)$$

Now, we demonstrate how the global SBP operator $\mathbf{D}_{x_i}^{s,g}$ mimics the IBP formula, i.e.,

$$\int_{\Omega} \left(\mathbf{V}^\top \frac{\partial \mathbf{U}}{\partial x_i} + \mathbf{U}^\top \frac{\partial \mathbf{V}}{\partial x_i} \right) \, d\Omega = \oint_{\Gamma} \mathbf{V}^\top \mathbf{U} n_{x_i} \, d\Gamma. \quad (23)$$

Discretizing the left-hand side of (23) using the global SBP operator $\mathbf{D}_{x_i}^{s,g}$ and the norm matrix \mathbf{P}_J^g , both of which are given in Definition 1, results in the equality

$$(\mathbf{v}^g)^\top \mathbf{P}_J^g \mathbf{D}_{x_i}^{s,g} \mathbf{u}^g + (\mathbf{u}^g)^\top \mathbf{P}_J^g \mathbf{D}_{x_i}^{s,g} \mathbf{v}^g = (\mathbf{v}^g)^\top \mathbf{E}_{x_i}^g \mathbf{u}^g, \quad (24)$$

where each term is an approximation to the corresponding term in the IBP formula (23).

In analogy to developing nonlinearly-stable (entropy-stable) numerical techniques for hyperbolic conservation laws, the convective term in (1) requires special care. In fact, while $D_{x_l}^{s,g}$ mimics the IBP rule, it does not mimic the telescoping property that is needed for the Lyapunov consistency analysis, namely (see Equation (13))

$$\int_{\Omega} \sum_{l=1}^{dim} \mathbf{w}^T \frac{\partial \mathbf{F}_{x_l}^{(c)}}{\partial x_l} d\Omega = \oint_{\Gamma} \sum_{l=1}^{dim} \mathfrak{F}_{x_l} n_{x_l} d\Gamma. \quad (25)$$

To mimic at the semi-discrete level (25), we can combine the SBP operator with Tadmor's two-point flux function [9] and their extension to SBP discretizations via the Hadamard formalism [19, 51]. The discrete operator that we require is given as

$$2D_{x_l}^{s,g} \circ F_{x_l}^{lc}(\mathbf{u}^g, \mathbf{u}^g) \mathbf{1} \approx \frac{\partial \mathbf{F}_{x_l}^{(c)}}{\partial x_l}(\mathbf{x}^g), \quad (26)$$

where \circ is the Hadamard product (entry-wise multiplication) between two matrices. Moreover $F_{x_l}^{lc}(\mathbf{u}^g, \mathbf{u}^g)$ is a symmetric matrix constructed from two point flux functions [9] and $\mathbf{1}$ is an appropriately sized vector of ones. The superscript "lc" in $F_{x_l}^{lc}(\mathbf{u}^g, \mathbf{u}^g)$ stands for "Lyapunov conservative". The details of this discrete operator on the left-hand side of (26) are presented in Appendix A.4. In the following theorem, we state that this operator mimics formula (25).

Theorem 3. *If the matrix $F_{x_l}^{lc}(\mathbf{u}^g, \mathbf{u}^g)$ is constructed from an entropy-consistent two-point flux function that is symmetric and satisfies the Tadmor shuffle condition [9] and $D_{x_l}^{s,g}$ is constructed such that $D_{x_l}^{s,g} \mathbf{1} = \mathbf{0}$ (see Appendix A.4 for more details on both of these points), then for the class of diagonal norm SBP operators with diagonal $E_{x_l}^g$ the following holds:*

$$2(\mathbf{w}^g)^T P_J^g D_{x_l}^{s,g} \circ F_{x_l}^{lc}(\mathbf{u}^g, \mathbf{u}^g) \mathbf{1} = \bar{\mathbf{1}}^T \bar{E}_{x_l}^g \mathfrak{f}_{x_l}^g, \quad (27)$$

where the overbar notation means the scalar version of a matrix or a vector, i.e., $E_{x_l}^g = \bar{E}_{x_l}^g \otimes \mathbf{1}_r$, where r is the number of equations. Furthermore, the vector $\mathfrak{f}_{x_l}^g$ is the vector constructed from evaluating the Lyapunov flux \mathfrak{F}_{x_l} at the mesh nodes.

Proof. See Appendix A.4 for the proof. \square

Next, we present approximations to the variable coefficient second derivative that are SBP. To do so, we use two different global matrix difference operators that are not SBP but combined, result in an SBP discretization of the second derivative.

Definition 2. *Under the same conditions as in Definition 1 the SBP approximation to the second derivative used in this paper is given as*

$$D_{x_l}^{sc,g} \left[\hat{C}_{l,m}^g \right] D_{x_m}^{c,g} = (P_J^g)^{-1} \left(- (D_{x_l}^{c,g})^T P_J^g \left[\hat{C}_{l,m}^g \right] D_{x_m}^{c,g} + E_{x_l}^g \left[\hat{C}_{l,m}^g \right] D_{x_m}^{c,g} \right), \quad (28)$$

where $\left[\hat{C}_{l,m}^g \right]$ is a block diagonal matrix with the $\hat{C}_{l,m}$ evaluated at its mesh nodes along its diagonal. Moreover, the matrix difference operator $D_{x_l}^{sc,g}$ is called "the strong-conservation form" approximation to the derivative $\frac{\partial}{\partial x_l}$ and while the matrix difference operator $D_{x_l}^{c,g}$ is called "the chain rule form". Neither of these operators are SBP, and their construction is detailed in Appendix A.

The specific IBP formula that we wish to mimic with our discretization of the second derivative is (see also Equation (12))

$$\int_{\Omega} \mathbf{V}^T \frac{\partial}{\partial x_l} \left(\hat{C}_{l,m} \frac{\partial \mathbf{U}}{\partial x_m} \right) d\Omega = \oint_{\Gamma} \mathbf{V}^T \hat{C}_{l,m} \frac{\partial \mathbf{U}}{\partial x_m} n_{x_l} d\Gamma - \int_{\Omega} \frac{\partial \mathbf{V}^T}{\partial x_l} \hat{C}_{l,m} \frac{\partial \mathbf{U}}{\partial x_l} d\Omega. \quad (29)$$

Discretizing the left-hand side of (29) using our SBP operator and the norm matrix results in the following equality:

$$(\mathbf{v}^g)^\top \mathbf{D}_{x_l}^{sc,g} \mathbf{P}_J^g \left[\widehat{\mathbf{C}}_{l,m}^g \right] \mathbf{D}_{x_m}^{c,g} \mathbf{u}^g = (\mathbf{v}^g)^\top \mathbf{E}_{x_l}^g \left[\widehat{\mathbf{C}}_{l,m}^g \right] \mathbf{D}_{x_m}^{sc,g} \mathbf{u}^g - (\mathbf{v}^g)^\top (\mathbf{D}_{x_l}^{c,g})^\top \mathbf{P}_J^g \left[\widehat{\mathbf{C}}_{l,m}^g \right] \mathbf{D}_{x_m}^{c,g} \mathbf{u}^g, \quad (30)$$

where we see that each term is an approximation to the corresponding term in the IBP formula (29).

We now have all the relevant pieces to construct our semi-discrete form of (7),

$$\begin{aligned} \frac{d\mathbf{u}^g}{dt} = & \mathbf{r}^g - \sum_{l=1}^d 2\mathbf{D}_{x_l}^{s,g} \circ \mathbf{F}_{x_l}^{lc}(\mathbf{u}^g, \mathbf{u}^g) \mathbf{1} + \sum_{l,m=1}^d \mathbf{D}_{x_l}^{sc,g} \left[\widehat{\mathbf{C}}_{l,m}^g \right] \mathbf{D}_{x_m}^{c,g} \mathbf{u}^g \\ & + \mathbf{SAT}^{(bc)} + \mathbf{diss}^{(c)} + \mathbf{diss}^{(d)}, \end{aligned} \quad (31)$$

where $\mathbf{SAT}^{(bc)}$ contains the boundary SATs to weakly impose the boundary condition and $\mathbf{diss}^{(c)}$ and $\mathbf{diss}^{(d)}$ add interface dissipation for the convective and the diffusion terms, respectively; their construction is detailed in Appendix C. For our analysis, we note that $\mathbf{diss}^{(c)}$ and $\mathbf{diss}^{(d)}$ are constructed such that

$$(\mathbf{w}^g)^\top \mathbf{P}_J^g \mathbf{diss}^{(c)} \leq 0, \quad (\mathbf{w}^g)^\top \mathbf{P}_J^g \mathbf{diss}^{(d)} \leq 0. \quad (32)$$

We observe that system (31) can be recast in the following compact and general ODE notation:

$$\frac{d\mathbf{U}(t)}{dt} = \mathbf{F}(\mathbf{U}(t)). \quad (33)$$

The proof of the stability of the equilibrium points of the semi-discrete equations defined by equation (31) follows identically to that of the continuous equations. Thus, we need to derive the expression of the time rate of change of the discrete Lyapunov functional. The first step is multiplying through by the Lyapunov variables and discretely integrating in space, followed by the discrete counterparts to the steps in equations (9) through (15). We summarize the result in the following theorem, i.e., the analog of Theorem 1 presented for the analysis at the continuous level.

Theorem 4. *Consider the equilibrium point \mathbf{u}_{eq} of the semi-discrete equations defined by the ODE system (31). Furthermore, assume that the following conditions are met:*

1. $\mathbf{W}^\top \mathbf{R} \leq 0$,
2. V is convex and locally positive definite,
3. $\widehat{\mathbf{M}} + \widehat{\mathbf{M}}^\top \geq 0$,
4. Appropriate boundary conditions and associated $\mathbf{SAT}^{(bc)}$ can be found such that

$$-\sum_{l=1}^{dim} \bar{\mathbf{1}}^\top \bar{\mathbf{E}}_{x_l}^g \mathbf{f}_{x_l}^g + \sum_{l,m=1}^{dim} (\mathbf{w}^g)^\top \mathbf{E}_{x_l}^g \left[\widehat{\mathbf{C}}_{l,m}^g \right] \mathbf{D}_{x_m}^{sc,g} \mathbf{w}^g + (\mathbf{w}^g)^\top \mathbf{P}_J^g \mathbf{SAT}^{(bc)} \leq 0.$$

Then, defining the discrete Lyapunov functional

$$\tilde{v}^g \equiv \sum_{k=1}^K \bar{\mathbf{1}}^\top \bar{\mathbf{P}}^k \left[\bar{\mathbf{J}}^k \right] \mathbf{v}^k, \quad (34)$$

where the vector \mathbf{v}^k is the discrete version of the Lyapunov function at the nodes of the k^{th} element, we have the following stability result:

- If \tilde{v}^g is locally positive definite and $d\tilde{v}^g/dt : \mathbb{R}^r \rightarrow \mathbb{R}$ is negative definite, and $\|\mathbf{u}^g\| \rightarrow +\infty \Rightarrow \tilde{v}^g(\mathbf{u}) \rightarrow +\infty$, then $\mathbf{u}_{eq} = 0$ is globally asymptotically stable.

Proof. We mimic the steps at the continuous level and seek to construct a bound on the time-derivative of \mathbf{v}^g . Multiplying (31) by $(\mathbf{w}^g)^\top \mathbf{P}_J^g$ results in

$$\begin{aligned} (\mathbf{w}^g)^\top \mathbf{P}_J^g \frac{d\mathbf{u}^g}{dt} &= (\mathbf{w}^g)^\top \mathbf{P}_J^g \mathbf{r}^g - \sum_{l=1}^{dim} 2 (\mathbf{w}^g)^\top \mathbf{P}_J^g \mathbf{D}_{x_l}^{s,g} \circ \mathbf{F}_{x_l}^{lc} (\mathbf{u}^g, \mathbf{u}^g) \mathbf{1} \\ &\quad + \sum_{l,m=1}^{dim} (\mathbf{w}^g)^\top \mathbf{P}_J^g \mathbf{D}_{x_l}^{sc,g} \left[\widehat{\mathbf{C}}_{l,m}^g \right] \mathbf{D}_{x_m}^{c,g} \mathbf{u}^g \\ &\quad + (\mathbf{w}^g)^\top \mathbf{P}_J^g \mathbf{SAT}^{(bc)} + (\mathbf{w}^g)^\top \mathbf{P}_J^g \mathbf{diss}^{(c)} + (\mathbf{w}^g)^\top \mathbf{P}_J^g \mathbf{diss}^{(d)}. \end{aligned} \quad (35)$$

The temporal term reduces as follows:

$$\begin{aligned} (\mathbf{w}^g)^\top \mathbf{P}_J^g \frac{d\mathbf{u}^g}{dt} &= \sum_{j=1}^{N^{dim}} \overline{\mathbf{P}}_J^g(j,j) \mathbf{w}^g(i,:)^\top \frac{d\mathbf{u}^g(i,:)}{dt} = \sum_{j=1}^{N^{dim}} \overline{\mathbf{P}}_J^g(j,j) \frac{d\mathbf{v}^g(i)}{dt} \\ &= \overline{\mathbf{I}}^\top \overline{\mathbf{P}}_J^g \frac{d\mathbf{v}^g}{dt}, \end{aligned} \quad (36)$$

where $\overline{\mathbf{I}}$ is a vector of ones of size N^{dim} (i.e., the number of nodes in the domain, N , to the power dim) and the bar over $\overline{\mathbf{P}}_J^g$ signifies the $N^{dim} \times N^{dim}$ version of this matrix. Furthermore, the notation $\mathbf{u}^k(i,:)$ means the $r \times 1$ portion of \mathbf{u}^g at the i^{th} node. The inviscid terms are recast with the help of Theorem 3, while the diffusion terms are recast using (28). Thus, Equation (35) becomes

$$\begin{aligned} \overline{\mathbf{I}}^\top \overline{\mathbf{P}}_J^g \frac{d\mathbf{v}^g}{dt} &= (\mathbf{w}^g)^\top \mathbf{P}_J^g \mathbf{r}^g - \sum_{l=1}^{dim} \overline{\mathbf{I}}^\top \overline{\mathbf{E}}_{x_l}^g \mathbf{f}_{x_l}^g \\ &\quad + \sum_{l,m=1}^{dim} (\mathbf{w}^g)^\top \left(-(\mathbf{D}_{x_l}^{c,g})^\top \mathbf{P}_J^g \left[\widehat{\mathbf{C}}_{l,m}^g \right] \mathbf{D}_{x_m}^{c,g} + \mathbf{E}_{x_l}^g \left[\widehat{\mathbf{C}}_{l,m}^k \right] \mathbf{D}_{x_m}^{c,g} \right) \mathbf{w}^g \\ &\quad + (\mathbf{w}^g)^\top \mathbf{P}_J^g \mathbf{SAT}^{(bc)} + (\mathbf{w}^g)^\top \mathbf{P}_J^g \mathbf{diss}^{(c)} + (\mathbf{w}^g)^\top \mathbf{P}_J^g \mathbf{diss}^{(d)}. \end{aligned} \quad (37)$$

By assumption $(\mathbf{w}^g)^\top \mathbf{P}_J^g \mathbf{r}^g \leq 0$. Moreover, we can recast the first part of the diffusion term as

$$- \sum_{l,m=1}^d (\mathbf{w}^g)^\top (\mathbf{D}_{x_l}^{c,g})^\top \mathbf{P}_J^g \left[\widehat{\mathbf{C}}_{l,m}^g \right] \mathbf{D}_{x_m}^{c,g} \mathbf{w}^g = \mathbf{z}^\top \hat{\mathbf{M}} \mathbf{z},$$

where $\mathbf{z} \equiv \left[(\mathbf{D}_{x_1}^{c,g} \mathbf{w}^g)^\top, \dots, (\mathbf{D}_{x_d}^{c,g} \mathbf{w}^g)^\top \right]^\top$. Thus, via the assumptions, we have $\mathbf{z}^\top \hat{\mathbf{M}} \mathbf{z} \leq 0$. In addition, $(\mathbf{w}^g)^\top \mathbf{P}_J^g \mathbf{diss}^{(c)} \leq 0$ and $(\mathbf{w}^g)^\top \mathbf{P}_J^g \mathbf{diss}^{(d)} \leq 0$. Therefore, dropping all negative semi-definite terms, expression (37) reduces to

$$\frac{d\tilde{v}^g}{dt} = \overline{\mathbf{I}}^\top \overline{\mathbf{P}}_J^g \frac{d\mathbf{v}^g}{dt} \leq - \sum_{l=1}^{dim} \overline{\mathbf{I}}^\top \overline{\mathbf{E}}_{x_l}^g \mathbf{f}_{x_l}^g + \sum_{l,m=1}^{dim} (\mathbf{w}^g)^\top \mathbf{E}_{x_l}^g \left[\widehat{\mathbf{C}}_{l,m}^k \right] \mathbf{D}_{x_m}^{sc,g} \mathbf{w}^g + (\mathbf{w}^g)^\top \mathbf{P}_J^g \mathbf{SAT}^{(bc)}. \quad (38)$$

The final results arises from the assumption on the interplay between terms on the right-hand side of (38). Moreover, \tilde{v}^g is locally positive since v^g is locally positive and $\frac{d\tilde{v}^g}{dt} = 0$ at the equilibrium point. Thus, the discrete Lyapunov function, v^g , can be converted into a Lyapunov functional, \tilde{v}^g , with the same properties. Therefore, we can apply Lyapunov's direct method and LaSalle's invariance principle [23, 24] to prove the stability statement for \mathbf{u}_{eq} . \square

5 Fully discrete schemes

The semi-discrete scheme (38) retains the stability properties of the original system of PDEs; however, these can be easily lost when discretizing the temporal term. Here, we consider a broader class of temporal discretization schemes that allow us to perform numerical time integration while retaining the stability properties of (38). Specifically, we use the explicit class of relaxation Runge–Kutta schemes [20, 21]. Relaxation Runge–Kutta schemes can be used to enforce conservation, dissipation, or other solution properties with respect to any convex function by adding a relaxation parameter that multiplies the Runge–Kutta update at each time step. The computational overhead is the solution of one additional nonlinear scalar algebraic equation for which a good initial guess is available. The analysis of these schemes in the context of Lyapunov consistent discretizations was first presented in [8]. Here, for completeness, we report the main results.

5.1 Relaxation Runge–Kutta methods

A general (explicit or implicit) Runge–Kutta method with s stages can be represented by its Butcher tableau [52],

$$\frac{\mathbf{c}}{\mathbf{b}^T} \Big| \mathbf{A}, \quad (39)$$

where $\mathbf{A} \in \mathbb{R}^{s \times s}$ and $\mathbf{b}, \mathbf{c} \in \mathbb{R}^s$. For the system of ODEs (31), a step from $\mathbf{U}^n \approx \mathbf{U}(t_n)$ to $\mathbf{U}^{n+1} \approx \mathbf{U}(t_{n+1})$, where $t_{n+1} = t_n + \Delta t$, is given by

$$\mathbf{Y}_i = \mathbf{U}^n + \Delta t \sum_{j=1}^s a_{ij} \mathbf{F}(t_n + c_j \Delta t, \mathbf{Y}_j), \quad i = 1, \dots, s, \quad (40a)$$

$$\mathbf{U}^{n+1} = \mathbf{U}^n + \Delta t \sum_{i=1}^s b_i \mathbf{F}(t_n + c_i \Delta t, \mathbf{Y}_i). \quad (40b)$$

Here, \mathbf{Y}_i are the stage values of the Runge–Kutta method, and \mathbf{F} is the right-hand side of the ODE system (31). To prevent confusion regarding the notation for these vectors of continuous functions, we note that uppercase \mathbf{U} , and \mathbf{F} are used for Runge–Kutta method in this section, as often used in the literature in our previous work [8]. In addition, for simplicity, we will make use of the shorthand

$$\mathbf{F}_i \equiv \mathbf{F}(t_n + c_i \Delta t, \mathbf{Y}_i), \quad \mathbf{F}_0 = \mathbf{F}(t_n, \mathbf{U}^n). \quad (41)$$

The basic idea to make a given Runge–Kutta method Lyapunov consistent (i.e., entropy stable in the framework of the compressible Euler and Navier–Stokes equations [21]) is to replace the update (40b) with

$$\mathbf{U}_\gamma^{n+1} = \mathbf{U}^n + \gamma_n \Delta t \sum_{i=1}^s b_i \mathbf{F}_i, \quad (42)$$

where γ_n is a real number called the relaxation parameter. The generalization to Lyapunov consistency is to enforce the condition

$$V(\mathbf{U}_\gamma^{n+1}) - V(\mathbf{U}^n) = \gamma_n \Delta t \sum_{i=1}^s b_i \langle V'(\mathbf{Y}_i), \mathbf{F}_i \rangle, \quad (43)$$

by finding a root γ_n of

$$q(\gamma) = V\left(\mathbf{U}^n + \gamma \Delta t \sum_{i=1}^s b_i \mathbf{F}_i\right) - V(\mathbf{U}^n) - \gamma \Delta t \sum_{i=1}^s b_i \langle V'(\mathbf{Y}_i), \mathbf{F}_i \rangle, \quad (44)$$

where V is the Lyapunov function or functional, and $\langle \cdot, \cdot \rangle$ denote the inner product inducing the norm $\| \cdot \|$. Note that $V'(\mathbf{Y}_i) = \mathbf{W}(\mathbf{Y}_i)$. Moreover, the direction

$$\mathbf{d}^n = \sum_{i=1}^s b_i \mathbf{F}_i, \quad (45)$$

and the estimate of the Lyapunov function change

$$e = \Delta t \sum_{i=1}^s b_i \langle V'(\mathbf{Y}_i), \mathbf{F}_i \rangle \quad (46)$$

can be computed on the fly during the calculations required by the Runge–Kutta method and are not influenced by the procedure used to compute γ_n [21]. Hence, existing low-storage Runge–Kutta implementations can be used.

In equation (44), $q(\gamma = 1)$ can be interpreted as the energy production of the unmodified Runge–Kutta method. Indeed, $V(\mathbf{U}^{n+1}) - V(\mathbf{U}^n)$ is the Lyapunov change and e in (46) is the energy function change. If the weights of the underlying Runge–Kutta method are $b_i \geq 0$, then e has the same sign as the true time derivative of the Lyapunov function or functional, dV/dt . Hence, q can be seen as the temporal energy production. Thus, finding a root of q yields a scheme that is Lyapunov consistent. This is formally summarized in the following theorem that was introduced in [21] for convex functionals in the context of the compressible Euler and Navier–Stokes equations.

Theorem 5. *The method defined by (40a) and (42), where γ_n is a root of (44), is Lyapunov conservative. If the weights b_i are non-negative and $\gamma_n \geq 0$, then the method is Lyapunov dissipation preserving.*

The following corollary provides a crucial element for preserving any form of Lyapunov consistency when a system of ODEs, endowed with a Lyapunov function or functional, is integrated with a RRK method.

Corollary 1. *Any Lyapunov function of system (33) is also a Lyapunov function of the relaxation Runge–Kutta method defined by (40a) and (42) if the weights b_i are non-negative and γ_n is a root of (44) or $\gamma_n \geq 0$.*

The following theorem provides the formal order of accuracy of relaxation Runge–Kutta methods.

Theorem 6. *The local error for relaxation Runge–Kutta method satisfies*

$$\|V(\mathbf{U}_\gamma^{n+1}) - V(\mathbf{U}(t_n + \gamma\Delta t))\| = \mathcal{O}(\Delta t^{p+1}), \quad (47a)$$

$$\|\mathbf{U}_\gamma^{n+1} - \mathbf{U}(t_n + \gamma\Delta t)\| = \mathcal{O}(\Delta t^{p+1}), \quad (47b)$$

where p is the order of the underlying Runge–Kutta method.

Proof. The error estimates are proven in [20, 21]. □

It is known that Runge–Kutta schemes can produce spurious solutions which, despite being non-oscillatory, are not solutions to the original differential equation [53, 54]. In the terminology of Iserles [55] such methods are not regular. In some circumstances, Newell [56], Brezzi et al. [57], and Griffiths et al. [54] found spurious solutions for certain values of the time step below the linearised stability limit where spurious invariant curves appear. The presence of spurious solutions may affect computations in that, although the fixed point of the continuous problem is globally asymptotically stable, they generally restrict the range of initial data that are attracted to it [54]. In the following, we state the main results that assure that the relaxation Runge–Kutta schemes do not produce spurious solutions. If we define a generic time marching method as

$$\mathbf{U}^{n+1} = \Phi(\mathbf{U}^n),$$

then a fixed point is a discrete solution, \mathbf{U}^n , such that $\Phi(\mathbf{U}^n) = \mathbf{U}^n$, and therefore, $\mathbf{U}^{n+1} = \mathbf{U}^n$. We define the set of fixed points of a time marching method as

$$E_{\Delta t} \equiv \{\mathbf{U}^n \in \mathbb{R}^l \mid \Phi(\mathbf{U}^n) = \mathbf{U}^n\},$$

where l is the number of equations in the ODE system. Similarly, the set of equilibrium points of the ODE is defined as

$$E \equiv \{\mathbf{U} \in \mathbb{R}^l \mid \mathbf{F}(\mathbf{U}) = 0\}.$$

Note that for the set of fixed point of the time marching scheme we use the subscript Δt because it may be a function of the time step [53].

For immediate use, we define a strict Lyapunov function for the ODE system as one whereby the equalities in

$$\frac{dV}{dt} = \mathbf{W}^T \mathbf{F} \leq 0$$

only holds on the set E . This implies that for $t_2 > t_1$

$$V(\mathbf{U}(t_2)) \leq V(\mathbf{U}(t_1)), \quad (48)$$

where the equality holds only if $\mathbf{U} \in E$.

Similarly, we define a strict discrete Lyapunov function as one that satisfies

$$V(\mathbf{U}_\gamma^{n+1}) \leq V(\mathbf{U}_\gamma^n), \quad (49)$$

where the equality holds for $\mathbf{U}^n \in E_{\Delta t}$.

Our first task is to determine the conditions such that $E_{\Delta t} = E$ for the relaxation Runge–Kutta method. The following result is due to Iserles [55] (see Theorem 3).

Lemma 1. $E \subseteq E_{\Delta t}$.

In the subsequent analysis we require that γ_n is positive; the following theorem (proven in [21]) states the conditions required for γ_n to be positive.

Theorem 7. For all, at least second order accurate, Runge–Kutta schemes and sufficiently small Δt , if $V''(\mathbf{U}^n) \langle \mathbf{F}_0, \mathbf{F}_0 \rangle > 0$, where $\mathbf{F}_0 = \mathbf{F}(\mathbf{U}^n)$, $q(\gamma_n)$ (44) has a positive root, i.e., $\gamma_n > 0$.

Remark 2. The statement $V''(\mathbf{U}^n) \langle \mathbf{F}_0, \mathbf{F}_0 \rangle > 0$ requires that $\mathbf{F}_0 \neq 0$, which is automatically satisfied for models away from their equilibrium. This makes $V''(\mathbf{U}^n) > 0$ the only requirement we need to satisfy.

Remark 3. At equilibrium points, $\mathbf{F}_0 = 0$. Thus, we require that $V''(\mathbf{U}^n) \langle \mathbf{F}_i, \mathbf{F}_i \rangle > 0$ for an intermediate step i , where $\mathbf{F}_i = \mathbf{F}(\mathbf{Y}_i)$, since they are non-zero by Taylor’s expansion around t_n [21].

In order to guarantee $\gamma_n > 0$ (Remark 2), we restrict our choice of Lyapunov functions, V , that satisfy $\frac{\partial^2 V}{\partial \mathbf{U}^2}(\mathbf{U}^n) > 0$, i.e., convex Lyapunov functions. This choice is obviously model dependent. Furthermore, as highlighted at the beginning of this section, the convexity of V is also required to ensure a one-to-one map between the state variables, \mathbf{U} , and the Lyapunov variables, \mathbf{W} .

Theorem 8. If the weights of the RRK method, $b_i > 0$, and $\gamma_n > 0$ then $E_{\Delta t} = E$.

Proof. The conditions such that $E_{\Delta t} = E$ are proven in [8]. □

6 Numerical Results

In this section, we numerically verify the accuracy and Lyapunov-consistency properties of the new discretizations by solving a dimerization problem. Dimerization is a fundamental concept in chemistry that plays a crucial role in various chemical processes and systems. It involves the combination of two identical or similar molecules to form a dimer through the formation of chemical bonds. A dimer is a molecular entity consisting of two monomers held together by chemical bonds.

Consider the reversible dimerization reaction



where monomers P dimerize at rate k_f , and dimers Q dissociate at rate k_r . The convection-diffusion-reaction dynamics of the local concentrations of monomers and dimers at position $x \in \Omega$ and time $t > 0$ is governed by

$$\frac{\partial}{\partial t} P = d_P \nabla^2 P - \boldsymbol{\alpha} \cdot \nabla P - 2k_f P^2 + 2k_r Q, \quad (51a)$$

$$\frac{\partial}{\partial t} Q = d_Q \nabla^2 Q - \boldsymbol{\beta} \cdot \nabla Q + k_f P^2 - k_r Q, \quad (51b)$$

where the positive constants d_P and d_Q are the monomers and dimers diffusion coefficients, respectively. The quantities $\boldsymbol{\alpha}$ and $\boldsymbol{\beta}$ are the velocity field vectors. The symbol $\Omega \subset \mathbb{R}^{dim}$ indicates a bounded domain with piecewise smooth boundary, Γ . At the boundary, periodic boundary conditions are used. The general initial conditions are give by $(P, Q)(x, 0) = (P_0, Q_0)(x)$ with $x \in \Omega$. We assume the dispersal strategy of the monomers and dimers only differs in their reaction rate, i.e., $d_P = d_Q = d$, and $\boldsymbol{\alpha} = \boldsymbol{\beta} = \mathbf{a}$.

Shear [58] demonstrated the existence of the Lyapunov function for homogeneous chemical reaction, such as the reversible dimerization reaction (50). He proved that the equilibrium point, $\mathbf{U}_{eq} = [P_{eq}, Q_{eq}]^T$, is globally asymptotically stable by using the following Lyapunov function

$$V(P, Q) = P \ln(P/P_{eq}) - P + P_{eq} + Q \ln(Q/Q_{eq}) - Q + Q_{eq}. \quad (52)$$

The Lyapunov functional for system (51) is obtained by integrating in space the Lyapunov function (52),

$$\tilde{V} \equiv \int_{\Omega} V d\Omega. \quad (53)$$

The Lyapunov consistency presented in Section 2 requires defining a two-point flux function, \mathfrak{F} . For system (50), the components of the two-point flux function read

$$F_{x_l}^{lc}(U_1, U_2) = a_{x_l} \mathbf{U}_{eq} \left[\left[\frac{\mathbf{U}}{\mathbf{U}_{eq}} \right] \right]_{\log}, \quad l = 1, \dots, dim, \quad (54)$$

with the logarithmic average given by

$$\left[\left[\frac{\mathbf{U}}{\mathbf{U}_{eq}} \right] \right]_{\log} = \frac{\frac{U_1}{U_{eq}} - \frac{U_2}{U_{eq}}}{\log \frac{U_1}{U_{eq}} - \log \frac{U_2}{U_{eq}}}, \quad (55)$$

where $\mathbf{U}_1 = [P_1, Q_1]$, $\mathbf{U}_2 = [P_2, Q_2]$, and the subscripts 1 and 2 indicate the two states needed for the two-point flux function.

6.1 Convergence Study

In this section, we aim to assess the order of accuracy of the proposed fully-discrete schemes by applying the method of manufactured solution (MMS) [59]. Here, we use the MMS to study the order of convergence of our new schemes applied to the convection-diffusion-reaction system (51) that models reversible dimerization chemical reactions.

The computational domain is a cube $\Omega = [0, 2\pi]^3$, where the following manufactured solution is used for the convergence study:

$$P = Q = \prod_{i=1,2,3} f_i(x_i, t) \text{ where } f_i(x_i, t) = 1.25 + 0.75 \sqrt{\cos(-\pi t + \pi x_i)}. \quad (56)$$

The final time of the simulation is set to $T_f = 1$. We run the convergence study with initial local concentrations of monomers and dimers as $P_0 = 10$ for monomers and $Q_0 = 1$ for dimers, respectively. The dimerization rate of monomers is set to $k_f = 10$, and the dissociation rate of dimers is set to $k_r = 1$. The diffusion coefficient d is fixed at 0.05, and the velocity field vector \mathbf{a} is set to the unit vector $\mathbf{1}$.

The convergence rates for the discrete error norms L^1 , L^2 , and L^∞ , defined in Appendix F, corresponding to second- ($p = 1$), third- ($p = 2$), fourth- ($p = 3$), and fifth-order ($p = 4$) accurate fully-discrete algorithms, are shown in Table 1. The solution polynomial degree p of the DG SBP-SAT operator used in the spatial discretization and the number of cells K in the computational mesh are shown in the table. In addition, we listed the relaxation Runge–Kutta time integration methods that are used to evolve the system of ODEs arising from the DG SBP-SAT spatial discretization [60]. We observe that numerical schemes with even-degree DG solution polynomials exhibit an L^2 convergence rate of approximately $p + 1$. In contrast, those with odd-degree DG polynomials converge at a higher rate. A similar pattern is seen for the L^1 and L^∞ error norms, except the $p = 1$ scheme in the case of the L^∞ norm.

Table 1: Convergence study for the convection-diffusion-reaction dynamics of the dimerization chemical reaction model using Lyapunov consistent DG SBP-SAT schemes with different solution polynomial degrees, p , and relaxation Runge–Kutta methods.

p	RK Method	K	L^1 Error	L^1 Rate	L^2 Error	L^2 Rate	L^∞ Error	L^∞ Rate
1	ERK(8,2)	512	7.99854e-01	-	9.56101e-01	-	3.18092e+00	-
		4,096	3.56431e-01	1.166	4.23122e-01	1.176	1.27381e+00	1.320
		32,768	1.09019e-01	1.709	1.27223e-01	1.734	3.72503e-01	1.774
		262,144	2.78390e-02	1.969	3.22426e-02	1.980	9.07434e-02	2.037
		2,097,152	6.87503e-03	2.018	8.05057e-03	2.002	2.20967e-02	2.038
2	BSRK(4,3)-3(2) pair	1,728	1.14981e-01	-	1.32592e-01	-	4.56714e-01	-
		13,824	8.51894e-03	3.755	8.85260e-03	3.905	4.23364e-02	3.431
		110,592	9.15459e-04	3.218	8.82595e-04	3.326	4.77381e-03	3.149
		884,736	1.09862e-04	3.059	1.07194e-04	3.042	5.92147e-04	3.011
		7,077,888	1.35060e-05	3.024	1.34799e-05	2.991	7.30730e-05	3.019
3	RK(4,4)	4,096	4.95896e-03	-	5.64148e-03	-	2.87246e-02	-
		32,768	5.03612e-04	3.299	5.33964e-04	3.401	3.10829e-03	3.208
		262,144	2.93424e-05	4.101	2.83613e-05	4.235	1.81243e-04	4.100
		2,097,152	1.28045e-06	4.518	1.16181e-06	4.609	7.75138e-06	4.547
		16,777,216	4.61820e-08	4.793	4.12820e-08	4.815	2.72962e-07	4.828
4	BSRK(8,5)-4(5) pair	8,000	7.35452e-04	-	8.41095e-04	-	6.28798e-03	-
		64,000	2.34012e-05	4.974	2.62451e-05	5.002	2.10179e-04	4.903
		512,000	7.20832e-07	5.021	7.63498e-07	5.103	6.37179e-06	5.044
		4,096,000	2.19966e-08	5.034	2.34475e-08	5.025	2.07971e-07	4.937
		32,768,000	6.80908e-10	5.014	7.33225e-10	4.999	6.70438e-09	4.955

Finally, we study the time-dependent coefficients for the diffusion terms in the same PDE model (51). For this purpose, the monomers and dimers diffusion coefficients d_P and d_Q are multiplied by $C_{fact} = 1 + 0.5 \sin(2\pi t)$, where t is the time. The results are shown in Table 2. We observe similar orders of accuracy to those reported for the previous case, where the diffusion coefficients remained constant over time.

Table 2: Convergence study for the convection-diffusion-reaction dynamics of the dimerization chemical reaction model using Lyapunov consistent DG SBP-SAT schemes with different solution polynomial degrees, p , and relaxation Runge–Kutta methods. The diffusion coefficients $C_{l,m}$ are time-dependent.

p	RK Method	K	L^1 Error	L^1 Rate	L^2 Error	L^2 Rate	L^∞ Error	L^∞ Rate
1	ERK(8,2)	512	7.95096e-01	-	9.51325e-01	-	3.20918e+00	-
		4,096	3.43179e-01	1.212	4.06416e-01	1.227	1.20634e+00	1.412
		32,768	1.05092e-01	1.707	1.22263e-01	1.733	3.58101e-01	1.752
		262,144	2.69018e-02	1.965	3.10639e-02	1.977	8.77128e-02	2.030
		2,097,152	6.64138e-03	2.018	7.75579e-03	2.009	2.13368e-02	2.039
2	BSRK(4,3)-3(2) pair	1,728	1.11522e-01	-	1.28893e-01	-	4.55491e-01	-
		13,824	8.43921e-03	3.724	8.75667e-03	3.880	4.17861e-02	3.446
		110,592	9.13462e-04	3.208	8.80679e-04	3.314	4.75647e-03	3.135
		884,736	1.09778e-04	3.057	1.07145e-04	3.039	5.91121e-04	3.008
		7,077,888	1.35018e-05	3.023	1.34784e-05	2.991	7.30127e-05	3.017
3	RK(4,4)	4,096	4.85403e-03	-	5.51374e-03	-	2.79356e-02	-
		32,768	4.95293e-04	3.293	5.24052e-04	3.395	3.07503e-03	3.183
		262,144	2.91624e-05	4.086	2.81495e-05	4.219	1.80249e-04	4.093
		2,097,152	1.27850e-06	4.512	1.15982e-06	4.601	7.73758e-06	4.542
		16,777,216	4.61633e-08	4.792	4.12647e-08	4.813	2.72839e-07	4.826
4	BSRK(8,5)-4(5) pair	8,000	7.33054e-04	-	8.39935e-04	-	6.29025e-03	-
		64,000	2.34562e-05	4.966	2.62946e-05	4.997	2.10260e-04	4.903
		512,000	7.21108e-07	5.024	7.63691e-07	5.106	6.37183e-06	5.044
		4,096,000	2.19973e-08	5.035	2.34481e-08	5.025	2.07940e-07	4.937
		32,768,000	6.80907e-10	5.014	7.33227e-10	4.999	6.76091e-09	4.943

6.2 Chemical reaction for the reversible dimerization model

To verify numerically the Lyapunov consistency properties of the algorithms, we compute the spatio-temporal evolution of the solution of the system (51) and monitor the convergence to the equilibrium point. The simulations are carried out using a spatially fourth-order accurate Lyapunov consistent DG SBP-SAT operator (i.e., the solution polynomial degree is $p = 3$). The time integration is performed using the RK 3(2) method of Bogacki–Shampine with adaptive time stepping [60].

To obtain the equilibrium condition of system (51), we use the rate equations that describe the local concentrations of monomers and dimers, i.e.,

$$P_t = -2k_f P^2 + 2k_r Q, \quad (57a)$$

$$Q_t = k_f P^2 - k_r Q. \quad (57b)$$

Then, the equilibrium condition reads

$$\frac{Q_{eq}}{P_{eq}^2} = \frac{k_f}{k_r}, \quad (58)$$

and the conservation relation $P + 2Q = P_0 + 2Q_0$ can be used to find the equilibrium point:

$$\mathbf{U}_{eq} = [P_{eq}, Q_{eq}] = \left[\frac{-k_r + \sqrt{k_r(8k_f(P_0 + 2Q_0) + k_r)}}{4k_f}, \frac{P_0 + 2Q_0 - P_{eq}}{2} \right]^T. \quad (59)$$

Here, we show the time evolution of the model (51) towards the equilibrium (59). The simulation is performed in a cube domain with a side length of 1 unit. This domain is discretized into 64 hexahedral cells in each coordinate direction. To investigate the impact of the reaction rate on the local concentrations of monomers and dimers, we distribute the monomers and dimers using a spherical harmonics shape located at the center of the cube, which is expressed in spherical coordinates as $HS = \tau(1 + 0.2(\sin(7\theta)\sin(4\phi)))$,

with a radius of $\tau = 0.30$. Within this region, the local concentrations of monomers and dimers are assigned specific values, $P_0 = 10$ for monomers and $Q_0 = 1$ for dimers. The local concentrations of monomers and dimers are assigned different values in the surrounding area, $P_0 = 0.1$ and $Q_0 = 0.1$, respectively. The dimerization rate of monomers is set to $k_f = 10$, and the dissociation rate of dimers is set to $k_r = 1$. The diffusion coefficient value is chosen as $d = 0.05$, and the velocity field vector is $\mathbf{a} = \mathbf{1}$.

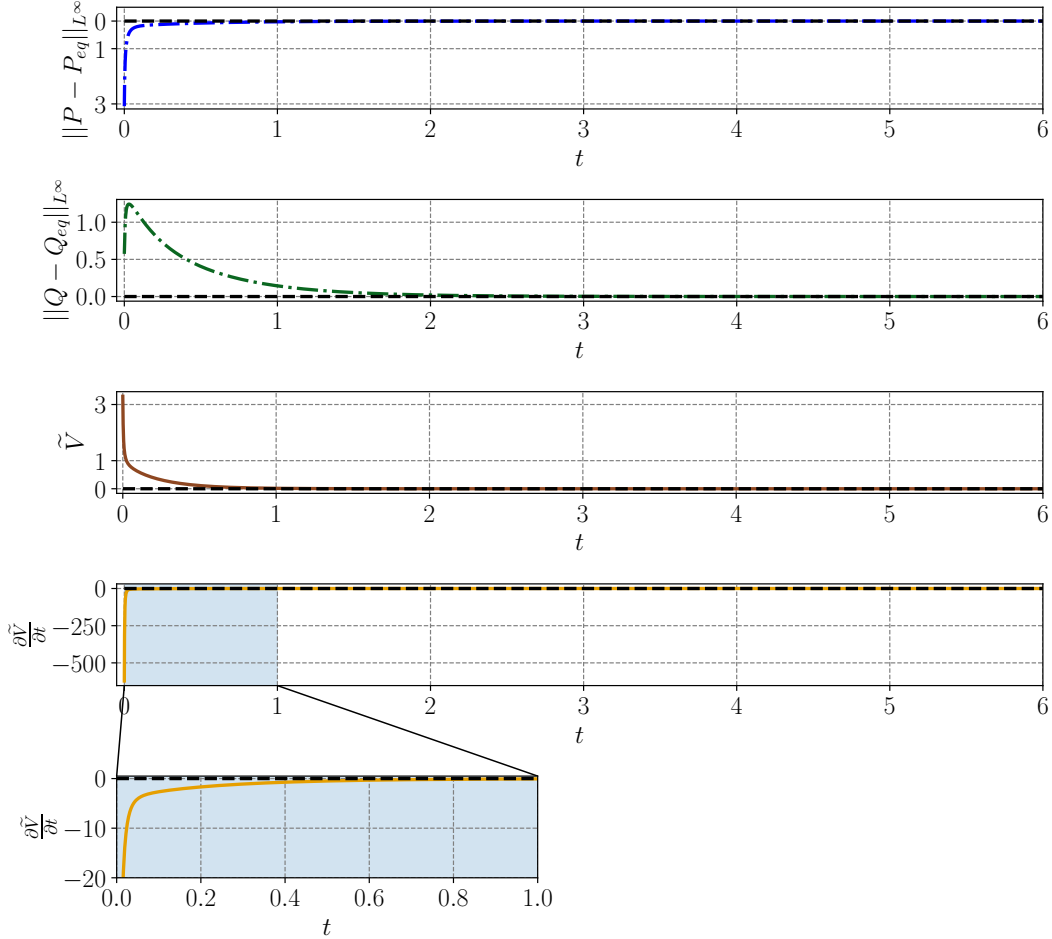
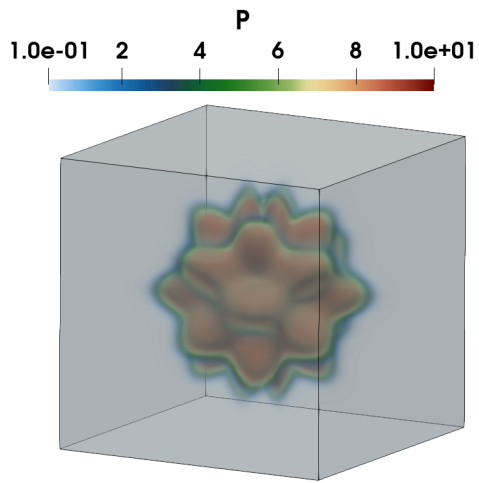
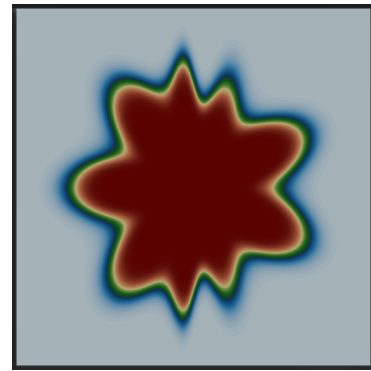


Fig. 2: Temporal evolution of the maximum norm of the difference of the solution (P, Q) and the equilibrium point (P_{eq}, Q_{eq}) , Lyapunov functional, \tilde{V} , and time derivative of the Lyapunov functional, $\frac{d\tilde{V}}{dt}$, for the chemical reaction model reversible dimerization.

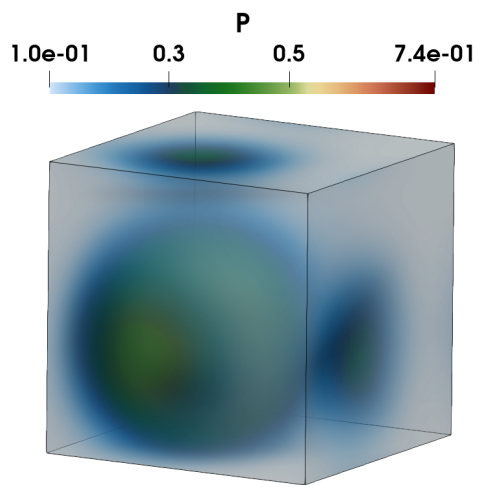
The first two one-dimensional plots at the top of Figure 2 illustrate the convergence of the solution to the equilibrium point $\mathbf{U}_{eq} = (P_{eq}, Q_{eq}) = (0.267912, 0.717767)$. Specifically, these plots show the temporal changes in the maximum norm of the difference between the solution (P, Q) , with respect to the equilibrium point (P_{eq}, Q_{eq}) . We observe that the solution gradually converges toward the equilibrium value over time. In addition, Figure 2 shows the time evolution of the Lyapunov functional, \tilde{V} , and its derivative, $d\tilde{V}/dt$, in the third and fourth one-dimensional plots, respectively. The spatiotemporal discretization preserves the convexity of \tilde{V} and the negative definiteness of $d\tilde{V}/dt$. These properties are crucial for establishing the global asymptotic stability of the equilibrium point.



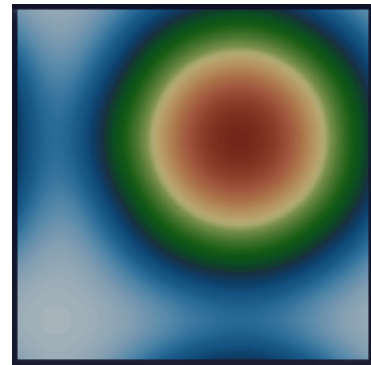
(a) $t = 0$



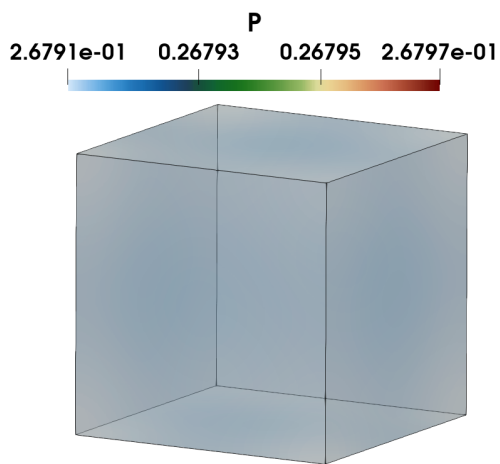
Vertical cross-section of the domain at $t = 0$



(b) $t = 0.127$



Vertical cross-section of the domain at $t = 0.127$.



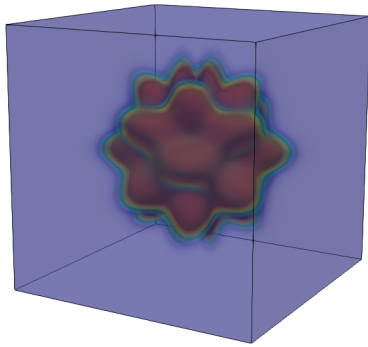
(c) $t = 6$



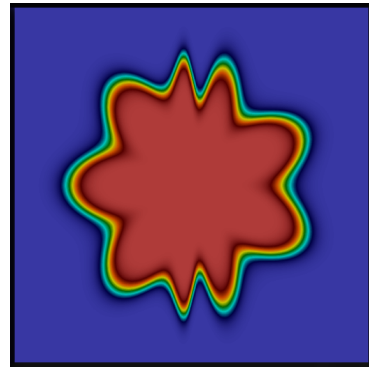
Vertical cross-section of the domain at $t = 6$.

Fig. 3: The local concentrations of monomers P at the initial transition at $t = 0$, the dampening stage at $t = 0.127$, and the final transition to a uniform state at $t = 6$.

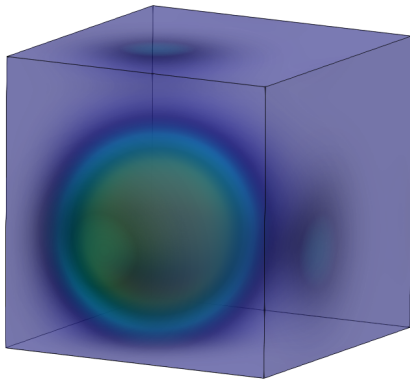
Figures 3 and 4 show the three-dimensional contour plots and vertical cross-sections illustrating the local concentrations of monomers P and dimers Q . The plots correspond to the initial time, $t = 0$, the dampening stage at $t = 0.127$, and the final uniform state at $t = 6$. These results demonstrate that the solution exhibits a persistent and consistent pattern, undergoing gradual reaction-diffusion-convection processes until it converges to a state of equilibrium characterized by uniform values in the whole domain, Ω . In addition, in Appendix E, we show the influence of mesh refinement on the convergence rate to the equilibrium point by conducting numerical simulations of the dimerization model with various numbers of cells.



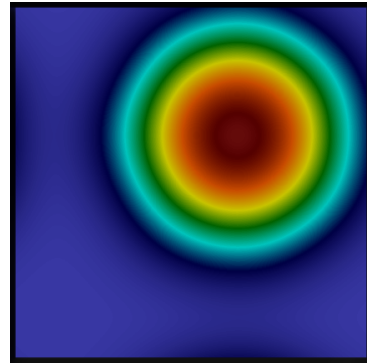
(a) $t = 0$



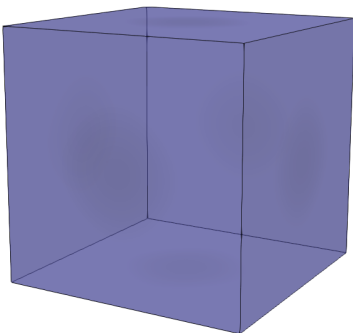
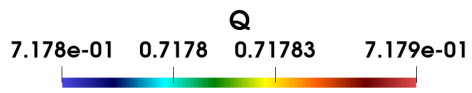
Vertical cross-section of the domain at $t = 0$



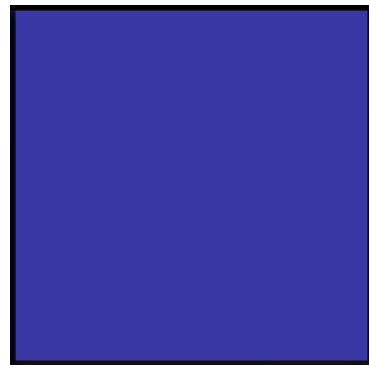
(b) $t = 0.127$



Vertical cross-section of the domain at $t = 0.127$.



(c) $t = 6$



Vertical cross-section of the domain at $t = 6$.

Fig. 4: The local concentrations of monomers Q at the initial transition at $t = 0$, the dampening stage at $t = 0.127$, and the final transition to a uniform state at $t = 6$.

6.3 Preserving Lyapunov stability with hp -nonconforming discretization

To demonstrate that the algorithms maintain the Lyapunov stability of the continuous model when using hp -adaptation [19], we conducted a numerical simulation of the dimerization model (51). A cubical computational domain with periodic boundary conditions on all six faces is used. We simulated this model using a grid with seven hexahedral elements in each coordinated direction, featuring a nonconforming interface, as shown in Figure 5. The grid is generated by assigning a random integer solution polynomial degree to each element, selected from the set $\{2, 3, 4, 5\}$. A second-order degree polynomial representation is used for all the boundary cell interfaces except those with periodic boundary conditions. All dissipation terms related to interface coupling [19, 43], including upwind and interior-penalty SATs, are turned off. The time integration is carried out using the BSRK(4,3)-3(2) pair method of Bogacki–Shampine with relaxation and adaptive time stepping based on error estimation [21, 60]. We maintain the same parameter values as in the previous section.

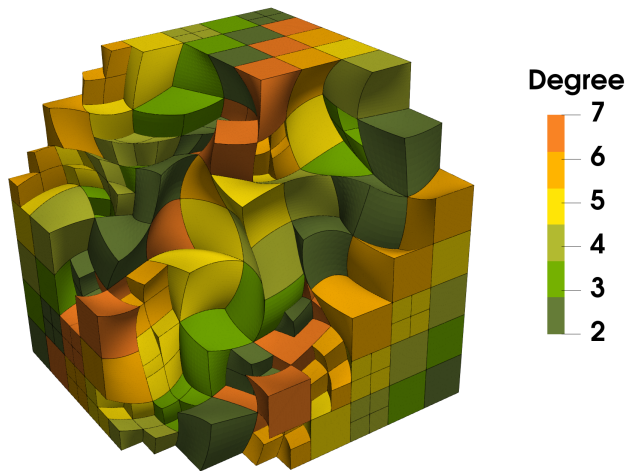


Fig. 5: Mesh structure with hp -adaptation. The colors indicating the solution polynomial degree distribution ($p = 2$ to $p = 7$) with one level of random mesh refinement.

We show the time evolution of the two-component model (51) and its Lyapunov functional in Figure 6. The top two one-dimensional plots illustrate the solution’s convergence to the equilibrium point $\mathbf{U}_{eq} = (P_{eq}, Q_{eq}) = (0.267912, 0.717767)$. These plots show the temporal changes in the maximum norm of the difference between the solution (P, Q) , with respect to the equilibrium point (P_{eq}, Q_{eq}) . We observe that the solution gradually converges toward the equilibrium point. Furthermore, the third and fourth plots show the time evolution of the Lyapunov functional, \tilde{V} , and its derivative, $d\tilde{V}/dt$, respectively. Also, in this case, we observe that the spatiotemporal discretization preserves the convexity of \tilde{V} and the negative definiteness of $d\tilde{V}/dt$.

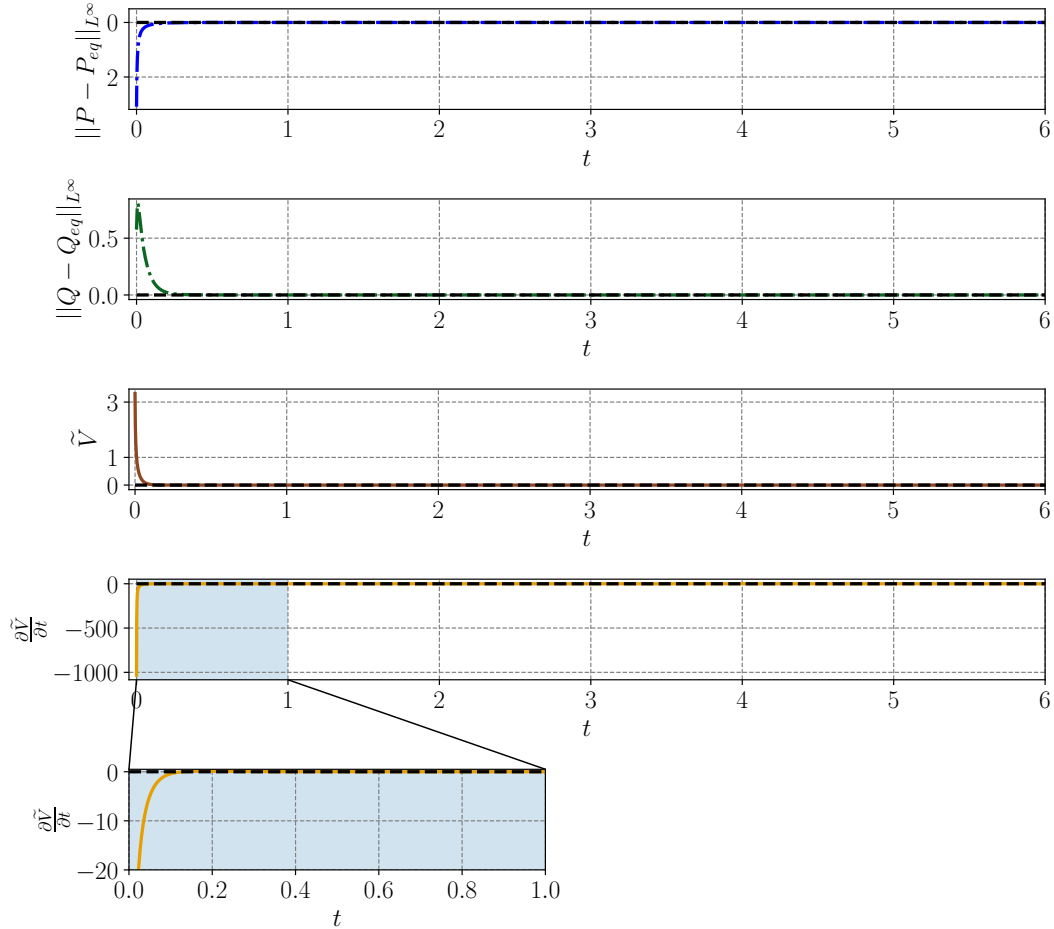


Fig. 6: Temporal evolution of the maximum norm of the difference of the solution (P, Q) and the equilibrium point (P_{eq}, Q_{eq}) , Lyapunov functional, \tilde{V} , and time derivative of the Lyapunov functional, $\frac{d\tilde{V}}{dt}$, for the chemical reaction model reversible dimerization with hp -nonconforming discretization.

To illustrate that the space and time discretizations and their coupling are indeed Lyapunov conservative, we compute the terms of the discrete Lyapunov functional balance (37). In Figure 7, we show the discrete-time rate of change of the Lyapunov functional, $d\tilde{V}/dt$, the discrete dissipation term, DT , and the discrete contribution of the reaction term, $\Xi = (\mathbf{w}^g)^T \mathbf{P}_j^g \mathbf{r}^g$. Additionally, we plot the instantaneous Lyapunov functional balance, $d\tilde{V}/dt + DT + \Xi$. The latter quantity is below machine's precision, numerically verifying the Lyapunov conservative property of the discretization.

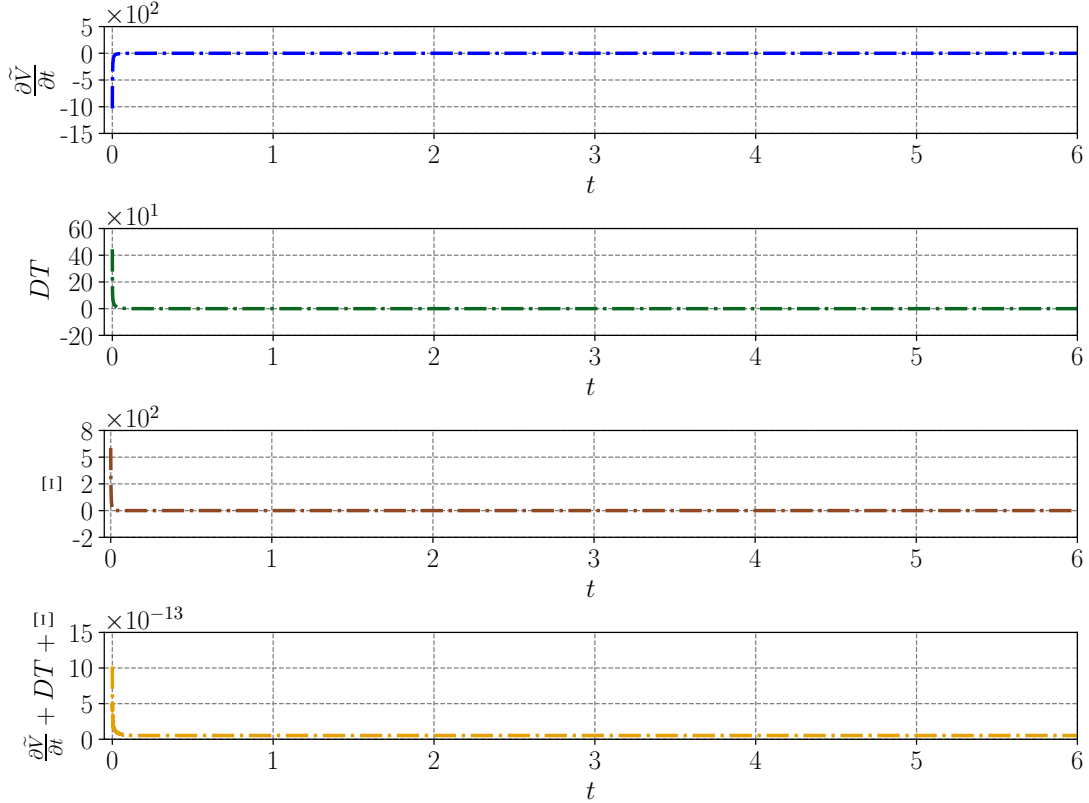


Fig. 7: Temporal evolution of the discrete-time rate of change of the Lyapunov functional, $d\tilde{V}/dt$, the discrete dissipation term, DT , the discrete contribution in the time derivative of Lyapunov functional of reaction term, Ξ , and the instantaneous Lyapunov functional balance, $d\tilde{V}/dt + DT + \Xi$.

7 Discussion

This work presents a general framework for constructing fully discrete Lyapunov-consistent discretizations for convection-diffusion-reaction PDE models. The proposed methods mimic the Lyapunov stability analysis at the fully discrete level. The spatial discretization is based on collocated discontinuous Galerkin operators with the summation-by-part property and the simultaneous approximation term technique for unstructured grids with tensor-product elements. In contrast, the temporal integration relies on relaxation Runge-Kutta methods. The proposed methodology is general and yields arbitrarily high-order accurate discretizations in space and time. To illustrate the capabilities of the proposed fully discrete algorithms, we solve a convection-diffusion-reaction system that models the evolving dynamics between monomer and dimer concentrations during the dimerization process. Finally, it is essential to highlight that the algorithms apply to a wide range of convection-reaction-diffusion equations, offering robust numerical tools that can provide valuable insights into the dynamics of complex systems.

Appendix A Global SBP operators for the first and second derivatives

In this section, we will first introduce SBP operators constructed in computational space and their properties. These are then extended to Cartesian derivatives by using a curvilinear mapping and a skew-symmetric splitting of the Cartesian derivatives. Next, the local Cartesian SBP operators are extended to global SBP operators by adding SATs to weakly couple elements at interfaces. To mimic the nonlinear

integration by parts that occurs for the convective terms, i.e.,

$$\int_{\Omega} \sum_{l=1}^d \mathbf{w}^T \frac{\partial \mathbf{U}}{\partial x_l} d\Omega = \int_{\Omega} \sum_{l=1}^d \frac{\partial V}{\partial x_m} d\Omega = \oint_{\Gamma} \sum_{l=1}^d V n_{x_m} d\Gamma,$$

we introduce the additional mechanics of Tadmor's two-point flux functions and its extension to SBP operators via the Hadamard formalism.

A.1 Computational space SBP operators

We start by constructing one-dimensional matrix difference SBP operators in a fixed computational reference space $\xi \in [-1, 1]$. The specific class of SBP operators we consider are of diagonal-norm, one-dimensional collocated SBP operators defined as follows:

Definition 3. *One-dimensional summation-by-parts operator for the first derivative: A matrix operator, $D_{\xi} \in \mathbb{R}^{N_{1d} \times N_{1d}}$, is a degree p SBP operator approximating the derivative $\partial/\partial\xi$ on the N_{1d} node nodal distribution $\boldsymbol{\xi} \equiv [-1, \xi_2, \dots, \xi_{N_{1d}-1}, 1]^T$, if*

1. $D_{\xi} \boldsymbol{\xi}^k = k \boldsymbol{\xi}^{k-1}$, $k = 0, \dots, p$;
2. $D_{\xi} \equiv P_{1d}^{-1} Q_{\xi}$, where the norm matrix, P_{1d} , is diagonal and symmetric positive definite;
3. $Q_{\xi} \equiv S_{\xi} + \frac{1}{2} E_{\xi}$, where $S_{\xi} = -S_{\xi}^T$, $E_{\xi} = E_{\xi}^T$;
4. $E_{\xi} \equiv \text{diag}(-1, 0, \dots, 0, 1) = \mathbf{e}_{N_{1d}}^T \mathbf{e}_{N_{1d}} - \mathbf{e}_1^T \mathbf{e}_1$, $\mathbf{e}_{N_{1d}} \equiv [0, \dots, 0, 1]^T$, and $\mathbf{e}_1 \equiv [1, 0, \dots, 0]^T$.

Moreover, $\boldsymbol{\xi}^k \equiv [-1^k, \xi_2^k, \dots, \xi_{N_{1d}-1}^k, 1^k]^T$, ξ_i is the ξ coordinate of the i^{th} node, and the convention that $\boldsymbol{\xi}^k = \mathbf{0}$ if $k < 0$ is used.

The critical property that we want these operators to mimic discretely is the IBP property, i.e.,

$$\int_{-1}^1 V^T \frac{\partial U}{\partial \xi} d\xi - \int_{-1}^1 V \frac{\partial U}{\partial \xi} d\xi = VU|_{-1}^1. \quad (\text{A1})$$

Given two scalar functions $U, V \in L^2(\xi)$, $\xi \in [-1, 1]$, we first note that the norm matrix, P_{1d} , is a high-order approximation to the L_2 inner product of the two functions evaluated at the N_{1d} node nodal distribution, i.e.,

$$\mathbf{v}^T P_{1d} \mathbf{u} \approx \int_{-1}^1 V U d\xi. \quad (\text{A2})$$

Using (A2) and the SBP derivative operators to discretize the left-hand side of (A1) results in the following equality:

$$\mathbf{v}^T P_{1d} D_{\xi_1} \mathbf{u} + \mathbf{u}^T P_{1d} D_{\xi} \mathbf{v} = \mathbf{v}^T E_{\xi} \mathbf{u} = \mathbf{v}(N) \mathbf{u}(N) - \mathbf{v}(1) \mathbf{u}(1), \quad (\text{A3})$$

where the notation $\mathbf{v}(i)$ means the i^{th} entry of the vector \mathbf{v} . Note that the terms in (A3) are high-order approximations individually to those in (A1). Moreover, the operators mimic the IBP rule in a telescoping sense in that the surface integral on the right-hand side of (A1) is split into individual surface contributions and, in the multidimensional case, into node-by-node contributions at surfaces. This property is important for the imposition of boundary conditions and minimal dissipation at interior element surfaces.

The one-dimensional SBP operators are extended to multiple dimensions and systems of equations using Kronecker products. Thus, for example, if $\dim = 2$, there are N_{1d} nodes in each direction, and there are r equations then the operators for the ξ_1 direction are

$$\begin{aligned} D_{\xi_1} &\equiv D_{\xi} \otimes I_{N_{1d}} \otimes I_r, & P &\equiv P_{1d} \otimes P_{1d} \otimes I_r, & Q_{\xi_1} &\equiv Q_{\xi} \otimes P_{1d} \otimes I_r, \\ E_{\xi_1} &\equiv (\mathbf{e}_{N_{1d}}^T \mathbf{e}_{N_{1d}} - \mathbf{e}_1^T \mathbf{e}_1) \otimes I_{N_{1d}} \otimes I_r = \left(R_{\xi_1}^{(N_{1d})} \right)^T P_{\xi_1}^{\perp} R_{\xi_1}^{(N_{1d})} - \left(R_{\xi_1}^{(1)} \right)^T P_{\xi_1}^{\perp} R_{\xi_1}^{(1)}, \\ R_{\xi_1}^{(N_{1d})} &\equiv \mathbf{e}_{N_{1d}}^T \otimes I_{N_{1d}} \otimes I_r, & R_{\xi_1}^{(1)} &\equiv \mathbf{e}_1^T \otimes I_{N_{1d}} \otimes I_r, & P_{\xi_1}^{\perp} &\equiv P_{1d} \otimes I_r, \end{aligned} \quad (\text{A4})$$

where the generic matrix \mathbf{I}_M is an $M \times M$ identity matrix. Extending the one-dimensional SBP operators preserves the SBP property. Consider the integration by parts rule in multiple dimensions, which now reads

$$\int_{\hat{\Omega}} \mathbf{V}^T \frac{\partial \mathbf{U}}{\partial \xi_l} d\hat{\Omega} + \int_{\hat{\Omega}} \mathbf{U}^T \frac{\partial \mathbf{V}}{\partial \xi_l} d\hat{\Omega} = \oint_{\hat{\Gamma}} \mathbf{V}^T \mathbf{U} n_{\xi_l} d\hat{\Gamma}, \quad (\text{A5})$$

where the computational domain in three dimensions is defined as $\hat{\Omega} \equiv [-1, 1]^3$ and n_{ξ_l} is the l^{th} component of the outward facing unit normal on the surface of the computational domain $\hat{\Gamma}$.

As in the one-dimensional case, the norm matrix, \mathbf{P} , defines a high-order discrete approximation to the L^2 inner product, i.e.,

$$\mathbf{v}^T \mathbf{P} \mathbf{u} \approx \int_{\hat{\Omega}} \mathbf{V}^T \mathbf{U} d\hat{\Omega}. \quad (\text{A6})$$

Discretizing the left-hand side of (A5) using (A6) and the multidimensional SBP operators results in the following equality,

$$\mathbf{v}^T \mathbf{P} \mathbf{D}_{\xi_l} \mathbf{u} + \mathbf{u}^T \mathbf{P} \mathbf{D}_{\xi_l} \mathbf{v} = \mathbf{v}^T \mathbf{E}_{\xi_l} \mathbf{u} = \mathbf{v}^T \left(\mathbf{R}_{\xi_l}^{(N_{1d})} \right)^T \mathbf{P}_{\xi_l}^\perp \mathbf{R}_{\xi_l}^{(N_{1d})} \mathbf{u} - \mathbf{v}^T \left(\mathbf{R}_{\xi_l}^{(1)} \right)^T \mathbf{P}_{\xi_l}^\perp \mathbf{R}_{\xi_l}^{(1)} \mathbf{u}. \quad (\text{A7})$$

A.2 Local Cartesian SBP operators

In the last section, we introduced SBP operators for fixed computational coordinates. In this section, we will use those operators to construct approximations to the first and the second derivatives in physical Cartesian coordinates that retain the SBP property. To do so consider the following expansion of the Cartesian derivatives in terms of the computational derivatives:

$$\frac{\partial}{\partial x_l} = \sum_{i=1}^{\dim} \frac{\partial \xi_i}{\partial x_l} \frac{\partial}{\partial \xi_i}, \quad \frac{\partial}{\partial x_l} = \sum_{i=1}^{\dim} J^{-1} \frac{\partial}{\partial \xi_i} J \frac{\partial \xi_i}{\partial x_l}, \quad (\text{A8})$$

where we denote the first form as the chain-rule form and the second as the strong-conservation form. The second form is derived from the first by multiplying through by the metric Jacobian J , using chain rule, and the metric identities

$$\sum_{l=1}^{\dim} \frac{\partial}{\partial \xi_l} \left(J \frac{\partial \xi_i}{\partial x_l} \right) = 0. \quad (\text{A9})$$

Averaging the two expansions (A8) of the Cartesian coordinates, we obtain a third expansion, which we denote as the skew-symmetric form, namely

$$\frac{\partial}{\partial x_l} = \frac{1}{2} \sum_{i=1}^{\dim} \left(\frac{\partial \xi_i}{\partial x_l} \frac{\partial}{\partial \xi_i} + J^{-1} \frac{\partial}{\partial \xi_i} J \frac{\partial \xi_i}{\partial x_l} \right). \quad (\text{A10})$$

Before constructing local Cartesian SBP approximations, we first define a norm matrix

$$\mathbf{P}_J \equiv \mathbf{P} [J], \quad (\text{A11})$$

where $[J]$ is a diagonal matrix with the metric Jacobian J along its diagonal. Since \mathbf{P} is a diagonal positive-definite matrix, and $[J]$ is a diagonal positive-definite matrix so too is \mathbf{P}_J .

To construct a Cartesian SBP operator, we use our computational SBP operators to discretize the skew-symmetric form of the Cartesian operators, that is

$$\mathbf{D}_{x_l}^s \equiv \frac{1}{2} \sum_{i=1}^{\dim} \left([J]^{-1} \mathbf{D}_{\xi_i} \left[J \frac{\partial \xi_i}{\partial x_l} \right] + [J]^{-1} \left[J \frac{\partial \xi_i}{\partial x_l} \right] \mathbf{D}_{\xi_i} \right), \quad (\text{A12})$$

where the superscript s reminds us that this is the skew-symmetric approximation (we will use a different form for the second derivative). Using the norm matrix, \mathbf{P}_J , we can construct the various matrices of the

skew-symmetric Cartesian SBP operator as

$$\mathbf{Q}_{x_l}^s \equiv \mathbf{P}_J \mathbf{D}_{x_l}^s = \frac{1}{2} \sum_{i=1}^{dim} \left(\mathbf{Q}_{\xi_i} \left[J \frac{\partial \xi_i}{\partial x_l} \right] + \left[J \frac{\partial \xi_i}{\partial x_l} \right] \mathbf{Q}_{\xi_i} \right). \quad (\text{A13})$$

Thus,

$$\begin{aligned} \mathbf{E}_{x_l} \equiv \mathbf{Q}_{x_l}^s + (\mathbf{Q}_{x_l}^s)^T &= \sum_{i=1}^{dim} \mathbf{E}_{\xi_i} \left[J \frac{\partial \xi_i}{\partial x_l} \right] = \\ &= \sum_{i=1}^{dim} \left((\mathbf{R}_{\xi_1}^{(N)})^T \mathbf{P}_{\xi_1}^\perp \mathbf{R}_{\xi_1}^{(N)} - (\mathbf{R}_{\xi_1}^{(1)})^T \mathbf{P}_{\xi_1}^\perp \mathbf{R}_{\xi_1}^{(1)} \right) \left[J \frac{\partial \xi_i}{\partial x_l} \right], \end{aligned} \quad (\text{A14})$$

and we can construct the skew symmetric part of the $\mathbf{Q}_{x_l}^s$ matrix as

$$\mathbf{S}_{x_l}^s \equiv \frac{1}{2} \sum_{i=1}^{dim} \left(\mathbf{S}_{\xi_i} \left[J \frac{\partial \xi_i}{\partial x_l} \right] + \left[J \frac{\partial \xi_i}{\partial x_l} \right] \mathbf{S}_{\xi_i} \right). \quad (\text{A15})$$

Note that \mathbf{E}_{x_l} does not have a superscript because it will appear for the second derivative operator as well.

Now, we demonstrate that these operators satisfy the SBP property. Discretizing the Cartesian version of IBP (A5) using the operators given in (A12)-(A14) yields the equality

$$\mathbf{v}^T \mathbf{P}_J \mathbf{D}_{x_l}^s \mathbf{u} + \mathbf{u}^T \mathbf{P}_J \mathbf{D}_{x_l}^s \mathbf{v} = \mathbf{v}^T \mathbf{E}_{x_l} \mathbf{u} = \sum_{i=1}^{dim} \mathbf{v}^T \left((\mathbf{R}_{\xi_i}^{(N_{1d})})^T \mathbf{P}_{\xi_i}^\perp \mathbf{R}_{\xi_i}^{(N_{1d})} - (\mathbf{R}_{\xi_i}^{(1)})^T \mathbf{P}_{\xi_i}^\perp \mathbf{R}_{\xi_i}^{(1)} \right) \left[J \frac{\partial \xi_i}{\partial x_l} \right] \mathbf{u}, \quad (\text{A16})$$

where we see that not only do we mimic IBP rule term-by-term and to high order, but the surface integrals are composed of individual contributions at surface nodes.

Before presenting the discrete operator for the second derivative, it is instructive to examine the IBP property that we intend to preserve, namely

$$\int_{\Omega} \mathbf{V}^T \frac{\partial}{\partial x_l} \left(\widehat{\mathbf{C}}_{l,m} \frac{\partial \mathbf{U}}{\partial x_m} \right) d\Omega = \oint_{\Gamma} \mathbf{V}^T \widehat{\mathbf{C}}_{l,m} \frac{\partial \mathbf{U}}{\partial x_m} n_{x_l} d\Gamma - \int_{\Omega} \frac{\partial \mathbf{V}^T}{\partial x_l} \widehat{\mathbf{C}}_{l,m} \frac{\partial \mathbf{U}}{\partial x_m} d\Omega. \quad (\text{A17})$$

While we could use the skew-symmetric formulation, we instead discretize using a combination of the strong conservation form, which is discretized as

$$\mathbf{D}_{x_l}^{sc} \equiv \sum_{i=1}^{dim} [J]^{-1} \mathbf{D}_{\xi_i} \left[J \frac{\partial \xi_i}{\partial x_l} \right], \quad (\text{A18})$$

and the chain rule form, which is discretized as

$$\mathbf{D}_{x_l}^c \equiv \sum_{i=1}^{dim} [J]^{-1} \left[J \frac{\partial \xi_i}{\partial x_l} \right] \mathbf{D}_{\xi_i}, \quad (\text{A19})$$

where the superscript *sc* and *c* are used to denote that these are discretizations for the strong conservation form and the chain-rule form, respectively. Note that these operators are not SBP by themselves. However, their combination for discretizing the second derivative satisfies the SBP property. Thus, we discretize the second derivative as

$$\mathbf{D}_{x_l}^{sc} \left[\widehat{\mathbf{C}}_{l,m} \right] \mathbf{D}_{x_m}^c \mathbf{u} \approx \frac{\partial}{\partial x_l} \left(\widehat{\mathbf{C}}_{l,m} \frac{\partial \mathbf{U}}{\partial x_m} \right), \quad (\text{A20})$$

where $\left[\widehat{\mathbf{C}}_{l,m}\right]$ is a block diagonal matrix with $\widehat{\mathbf{C}}_{l,m}$ evaluated at each node. Discretizing the left-hand side of (A17) using the operator (A20) and \mathbf{P}_J defined in (A11) gives the following equality:

$$\mathbf{v}^T \mathbf{P}_J \mathbf{D}_{x_l}^{sc} \left[\widehat{\mathbf{C}}_{l,m}\right] \mathbf{D}_{x_m}^c \mathbf{u} = \mathbf{v}^T \mathbf{E}_{x_l} \mathbf{u} - \mathbf{v}^T \left(\mathbf{D}_{x_l}^c\right)^T \left[\widehat{\mathbf{C}}_{l,m}\right] \mathbf{D}_{x_m}^c \mathbf{u}. \quad (\text{A21})$$

A.3 Global Cartesian SBP operators

In the previous section, we constructed Cartesian SBP operators that act at the element level and preserve the SBP property. However, to construct stability proofs of the theorems presented in Section 4, we need SBP operators over the entire set of elements used to discretize the domain Ω with boundary Γ . We can construct such global SBP operators by using appropriate SATs. In this section, we demonstrate the procedure using simple two-element examples, i.e., left and right elements denoted with the superscripts L and R , respectively.

For this purpose, we consider two elements with a common vertical surface. For simplicity of presentation, we consider that all coordinate systems are aligned, i.e., the Cartesian and computational coordinates are aligned within each element and are aligned between elements (we don't mean parallel, but rather that they generally point in the same direction). For simplicity of explanation but without loss of generality, suppose that the SBP operator $\mathbf{D}_{x_l}^{s,L}$ is applied to the vector \mathbf{u}^L , i.e., $\mathbf{D}_{x_l}^{s,L} \mathbf{u}^L$. Thus, we modify the Cartesian derivative of the left element, $\mathbf{D}_{x_l}^{s,L} \mathbf{u}^L$, with an interface SAT coupling it to the right element as follows:

$$\mathbf{D}_{x_l}^{s,L} \mathbf{u}^L + \mathbf{SAT}_L \approx \frac{\partial \mathbf{U}_L}{\partial x_m}, \quad (\text{A22})$$

where

$$\mathbf{SAT}^L \equiv -\frac{1}{2} \left(\mathbf{P}_J^L\right)^{-1} \left(\mathbf{R}_{\xi_1}^{(N_{1d})}\right)^T \mathbf{P}_{\xi_1}^\perp \left(\mathbf{R}_{\xi_1}^{(N_{1d})} \left[J \frac{\partial \xi_1}{\partial x_l} \right]_L \mathbf{u}_L - \mathbf{R}_{\xi_1}^{(1)} \left[J \frac{\partial \xi_1}{\partial x_l} \right]_R \mathbf{u}_R\right). \quad (\text{A23})$$

We proceed similarly for the right element and obtain

$$\mathbf{D}_{x_l}^{s,R} \mathbf{u}_R + \mathbf{SAT}_R \approx \frac{\partial \mathbf{U}_R}{\partial x_m}, \quad (\text{A24})$$

where

$$\mathbf{SAT}^R \equiv \frac{1}{2} \left(\mathbf{P}_J^R\right)^{-1} \left(\mathbf{R}_{\xi_1}^{(1)}\right)^T \mathbf{P}_{\xi_1}^\perp \left(\mathbf{R}_{\xi_1}^{(1)} \left[J \frac{\partial \xi_1}{\partial x_l} \right]_R \mathbf{u}_R - \mathbf{R}_{\xi_1}^{(N_{1d})} \left[J \frac{\partial \xi_1}{\partial x_l} \right]_L \mathbf{u}_L\right). \quad (\text{A25})$$

Now, we construct a global SBP operator over the two elements and obtain the following:

$$\mathbf{D}_{x_l}^{s,g} \equiv \overbrace{\left[\begin{array}{c} \mathbf{P}_J^L \\ \mathbf{P}_J^R \end{array} \right]}^{\equiv \mathbf{P}_J^g} \left(\overbrace{\left[\begin{array}{cc} \mathbf{S}_{x_l}^{s,L} & \mathbf{CT}_L \\ \mathbf{CT}_R & \mathbf{S}_{x_l}^{s,R} \end{array} \right]}^{\equiv \mathbf{S}_{x_l}^{s,g}} + \frac{1}{2} \overbrace{\left[\begin{array}{cc} \mathbf{E}_{x_l}^L - \mathbf{IS}_L & \\ & \mathbf{E}_{x_l}^R - \mathbf{IS}_R \end{array} \right]}^{\equiv \mathbf{E}_{x_l}^g} \right), \quad (\text{A26})$$

where $\mathbf{S}_{x_l}^{s,L/R}$ are constructed using (A15), and

$$\begin{aligned} \mathbf{CT}_L &\equiv \frac{1}{2} \left(\mathbf{R}_{\xi_1}^{(N_{1d})}\right)^T \mathbf{P}_{\xi_1}^\perp \mathbf{R}_{\xi_1}^{(1)} \left[J \frac{\partial \xi_1}{\partial x_l} \right]_R, \\ \mathbf{CT}_R &\equiv -\frac{1}{2} \left(\mathbf{R}_{\xi_1}^{(1)}\right)^T \mathbf{P}_{\xi_1}^\perp \mathbf{R}_{\xi_1}^{(N_{1d})} \left[J \frac{\partial \xi_1}{\partial x_l} \right]_L. \end{aligned} \quad (\text{A27})$$

We note that for consistent approximations the metric terms $\left[J \frac{\partial \xi_1}{\partial x_l} \right]_L$ and $\left[J \frac{\partial \xi_1}{\partial x_l} \right]_R$ are the same at the joined boundary points. Then, $\mathbf{CT}_R = -\mathbf{CT}_L$ and therefore $\mathbf{S}_{x_l}^{sc,g}$ is skew-symmetric. Finally,

$$\begin{aligned} \mathbf{IS}_L &\equiv \frac{1}{2} \left(\mathbf{R}_{\xi_1}^{(N_{1d})} \right)^T \mathbf{P}_{\xi_1}^\perp \mathbf{R}_{\xi_1}^{(N_{1d})} \left[J \frac{\partial \xi_1}{\partial x_l} \right]_L, \\ \mathbf{IS}_R &\equiv -\frac{1}{2} \left(\mathbf{R}_{\xi_1}^{(1)} \right)^T \mathbf{P}_{\xi_1}^\perp \mathbf{R}_{\xi_1}^{(1)} \left[J \frac{\partial \xi_1}{\partial x_l} \right]_R. \end{aligned} \quad (\text{A28})$$

We also note that the action of the \mathbf{IS} terms is to remove the contribution of the \mathbf{E}_x matrices at the interior interface so that the symmetric matrix $\mathbf{E}_{x_l}^g$ only contains terms that contribute to the boundaries of the two-element mesh.

This procedure can be applied at all interior interfaces and the resultant global operators preserve the SBP property and have the following matrix properties:

$$\mathbf{D}_{x_l}^{s,g} = (\mathbf{P}_J^g)^{-1} \mathbf{Q}_{x_l}^{s,g}, \quad \mathbf{Q}_{x_l}^{s,g} + (\mathbf{Q}_{x_l}^{s,g})^T = \mathbf{E}_{x_l}^g. \quad (\text{A29})$$

The matrix $\mathbf{E}_{x_l}^g$ is a surface integration matrix such that for M surfaces it has the following form,

$$\mathbf{E}_{x_l}^g \equiv \sum_{i=1}^M n_{\xi_{\Gamma_i}} \left(\mathbf{R}_{\xi_{\Gamma_i}} \right)^T \mathbf{P}_{\xi_{\Gamma_i}}^\perp \mathbf{R}_{\xi_{\Gamma_i}} \left[J \frac{\partial \xi_{\Gamma_i}}{\partial x_m} \right], \quad (\text{A30})$$

where Γ_i specifies the computational coordinate orthogonal to the i^{th} surface (i.e., in three dimensions Γ_i can be 1 or 2 or 3). For example, suppose the surface is orthogonal to ξ_1 and at the maximum of ξ_1 then $\mathbf{R}_{\xi_{\Gamma_i}} = \mathbf{R}_{\xi_1}^{(N)}$, $\mathbf{P}_{\xi_{\Gamma_i}}^\perp = \mathbf{P}_{\xi_1}^\perp$, and $\left[J \frac{\partial \xi_{\Gamma_i}}{\partial x} \right] = \left[J \frac{\partial \xi_1}{\partial x} \right]$.

We proceed in an identical manner for the approximation to the second derivative and in the same way as at the element level, we define two global matrices $\mathbf{D}_{x_l}^{sc,g}$ and $\mathbf{D}_{x_m}^{c,g}$ and construct the global SBP approximation to the second derivative as

$$\mathbf{D}_{x_l}^{sc,g} \left[\widehat{\mathbf{C}}_{l,m}^g \right] \mathbf{D}_{x_m}^{c,g} = (\mathbf{P}_J^g)^{-1} \left(-(\mathbf{D}_{x_l}^{c,g})^T \mathbf{P}_J^g \left[\widehat{\mathbf{C}}_{l,m}^g \right] \mathbf{D}_{x_m}^{c,g} + \mathbf{E}_{x_l}^g \left[\widehat{\mathbf{C}}_{l,m}^k \right] \mathbf{D}_{x_m}^{c,g} \right), \quad (\text{A31})$$

where the right-hand side decomposition demonstrates the SBP property of this operator.

A.4 Convective term: Tadmor's two-point flux functions and the Hadamard formalism

To mimic the continuous proof at the semi-discrete level, we need approximations to the convective terms that reduce to discrete surface integrals when discretely integrated against the Lyapunov variables. In particular, we rely on combining SBP operators with two-point flux functions of Tadmor [9]. The required mechanics are involved, and we attempt to convey all the details clearly. However, the interested reader is referred to the literature on entropy-stable methods.

To begin, we introduce the following scalar function, called Lyapunov potential,

$$\psi \equiv \mathbf{W}^T \mathbf{U} - V, \quad (\text{A32})$$

where \mathbf{W} , \mathbf{U} , and V are the Lyapunov variables, the conserved variables, and the Lyapunov function, respectively. Next, we introduce the two-point flux functions, \mathbf{F}^{lc} , that satisfies the following three conditions:

1. Consistency: $\mathbf{F}^{lc}(\mathbf{u}^L(j, :), \mathbf{u}^L(j, :)) = \mathbf{F}^{(c)}(\mathbf{u}^L(j, :))$,
2. Tadmor shuffle condition for the convective spatial flux terms [9],

$$\left(\mathbf{u}^L(i, :) - \mathbf{u}^R(j, :) \right)^T \mathbf{F}^{lc}(\mathbf{u}^L(i, :), \mathbf{u}^R(j, :)) = \psi^L(i) - \psi^R(j) \quad (\text{A33})$$

3. Symmetry: $\mathbf{F}^{lc}(\mathbf{u}^L(i, :), \mathbf{u}^R(j, :)) = \mathbf{F}^{lc}(\mathbf{u}^R(j, :), \mathbf{u}^L(i, :))$,

where \mathbf{u}^L and \mathbf{u}^R are the discrete solution vectors for an element to the left and right of an interface, respectively, with similar interpretations for \mathbf{w}^L , \mathbf{w}^R , $\boldsymbol{\psi}^L$, and $\boldsymbol{\psi}^R$, where the latter are constructed from the \mathbf{u} vectors using (A32). The notation, for example, $\mathbf{u}^L(i, :)$ means the $r \times 1$ solution vector at the i^{th} node where r is the number of equations in the PDE.

To achieve Lyapunov consistency, the approximations to the spatial derivatives of the convective flux are constructed such that the continuous Lyapunov analysis is mimicked in a term-by-term in the semi-discrete context. To this end, the approximation to the spatial derivatives has to be mimetic to a special case of the integration by parts, namely

$$\int_D \mathbf{Q}^T \frac{\partial \mathbf{G}}{\partial \chi} dD = \int_D \frac{\partial h}{\partial \chi} dD = \oint_B h n_\chi dB, \quad (\text{A34})$$

where where \mathbf{Q} and $\mathbf{G}(\mathbf{U})$ are vector valued functions, $h(\mathbf{U})$ is a scalar function, χ is some independent variable over the domain D with boundary B , and n_χ is the component of the outward facing unit normal in the χ direction. In the present analysis, \mathbf{Q} , $\mathbf{G}(\mathbf{U})$, and h play the role of the Lyapunov variables, \mathbf{W} , the convective fluxes, $\mathbf{F}_{x_m}^{(c)}$, or the conservative variables, \mathbf{U} , and the Lyapunov fluxes, \mathfrak{F}_{x_m} , or the Lyapunov function, V , respectively. Equation (A34) is referred to as a nonlinear IBP relation and the numerical operators that mimic this property discretely are called nonlinear SBP operators.

The nonlinear SBP operators constructed and used in this work to discretize the divergence of the convective and diffusive fluxes for the system of PDEs (1) satisfy the following approximations [61],

$$\begin{aligned} 2 \left(\mathbf{D}_{\xi_i} \left[J \frac{\partial \xi_i}{\partial x_l} \right]_k \right) \circ \mathbf{F}^{lc}(\mathbf{u}^k, \mathbf{u}^k) \mathbf{1} &\approx \left(\frac{\partial}{\partial \xi_i} \left(J \frac{\partial \xi_i}{\partial x_l} \mathbf{F}^{(c)} \right) + \mathbf{F}^{(c)} \frac{\partial}{\partial \xi_i} \left(J \frac{\partial \xi_i}{\partial x_l} \right) \right) \Big|_{C_k}, \\ 2 \left(\left[J \frac{\partial \xi_i}{\partial x_l} \right]_k \mathbf{D}_{\xi_i} \right) \circ \mathbf{F}^{lc}(\mathbf{u}^k, \mathbf{u}^k) \mathbf{1} &\approx \left(\frac{\partial}{\partial \xi_i} \left(J \frac{\partial \xi_i}{\partial x_l} \mathbf{F}^{(c)} \right) \right) \Big|_{C_k}, \end{aligned} \quad (\text{A35})$$

where \circ represents the Hadamard product (i.e., the entry-wise multiplication of two matrices), and the notation “ $(a)|_{C_k}$ ” indicates the vector constructed by evaluating the quantity a at the set of nodes C of the element k , i.e., C_k . The proofs of (A35) is given in [61] and follow in a straightforward manner from the Theorem 1 in [48]. The block diagonal matrix $\mathbf{F}^{lc}(\mathbf{u}^k, \mathbf{u}^k)$, for the k^{th} element having discrete solution vector \mathbf{u}^k , is constructed as

$$\mathbf{F}^{lc}(\mathbf{u}^k, \mathbf{u}^k) \equiv \begin{bmatrix} \text{diag}(\mathbf{F}^{lc}(\mathbf{u}^k(1, :), \mathbf{u}^k(1, :))) & \dots & \text{diag}(\mathbf{F}^{lc}(\mathbf{u}^k(1, :), \mathbf{u}^k(N_{1d}, :))) \\ \vdots & & \vdots \\ \text{diag}(\mathbf{F}^{lc}(\mathbf{u}^k(N_{1d}, :), \mathbf{u}^k(1, :))) & \dots & \text{diag}(\mathbf{F}^{lc}(\mathbf{u}^k(N_{1d}, :), \mathbf{u}^k(N_{1d}, :))) \end{bmatrix}, \quad (\text{A36})$$

where N_{1d}^{dim} (i.e., N_{1d} to the power dim) is the total number of nodes in the element k . Note that via the properties of \mathbf{F}^{lc} the matrix $\mathbf{F}^{lc}(\mathbf{u}^k, \mathbf{u}^k)$ is symmetric.

Our construction of a global nonlinear SBP operator follows identically as before, and we obtain the approximation [19, 48, 51, 61]

$$2\mathbf{D}_{x_l}^{s,g} \circ \mathbf{F}^{lc}(\mathbf{u}^g, \mathbf{u}^g) \mathbf{1} \approx \frac{\partial \mathbf{F}^{(c)}}{\partial x_l}(\mathbf{x}_g), \quad (\text{A37})$$

where the notation $\frac{\partial \mathbf{F}^{(c)}}{\partial x_l}(\mathbf{x}_g)$ means the vector that results from evaluating $\frac{\partial \mathbf{F}^{(c)}}{\partial x_l}$ at the mesh nodes. In addition, the resulting (global) nonlinear SBP operator satisfies the discrete counterpart of the nonlinear IBP rule (A34); see [19, 51, 61] and also Theorem 4.2 in [62].

For our discretization to result in a Lyapunov-consistent formulation, we need our global SBP operator to discretely satisfy the metric invariants (similarly to the entropy conservative and stable discretizations proposed in [19]), which are

$$\sum_{i=1}^{\text{dim}} \frac{\partial}{\partial \xi_i} \left(J \frac{\partial \xi_i}{\partial x_l} \right) = 0, \quad l = 1, \dots, \text{dim}. \quad (\text{A38})$$

The discrete counter-part to (A38) turns out to be [19, 63]

$$\mathbf{D}_{x_l}^{s,g} \mathbf{1} = 0. \quad (\text{A39})$$

To understand why, note that the SATs used to construct $\mathbf{D}_{x_l}^{s,g}$ in Appendix A.3 cancel for the constant vector. Thus, we have the following local statements

$$\sum_{i=1}^{dim} \mathbf{D}_{\xi_i} \left[J \frac{\partial \xi_i}{\partial x_l} \right] \mathbf{1} + \left[J \frac{\partial \xi_i}{\partial x_l} \right] \mathbf{D}_{\xi_i} = \sum_{i=1}^{dim} \mathbf{D}_{\xi_i} \left[J \frac{\partial \xi_i}{\partial x_l} \right] \mathbf{1} = 0. \quad (\text{A40})$$

In this work, the metric terms for conforming and non-conforming elements with mesh- (h -) and solution polynomial degree (p -) refinements are constructed to satisfy (A40) as reported in [19]. Therefore, (A39) holds.

We need one last theorem before we can show why the involved discretization of the convective terms mimics the continuous proof of the Lyapunov consistency. This theorem is given next.

Theorem 9. Consider an arbitrary matrix $\bar{\mathbf{A}}$ of size $N^{dim} \times N^{dim}$ and the matrix $\mathbf{F}^{lc}(\mathbf{u}^L, \mathbf{u}^R)$ constructed from a two-point flux function $\mathbf{F}^{lc}(\mathbf{u}^L(i, :), \mathbf{u}^R(j, :))$, that is symmetric and satisfies the Tadmor's shuffle condition [9]. Then, for $\mathbf{A} \equiv \bar{\mathbf{A}} \otimes \mathbf{1}_r$

$$(\mathbf{w}^L)^\top (\mathbf{A} \circ \mathbf{F}^{lc}(\mathbf{u}^L, \mathbf{u}^R)) \mathbf{1} - \mathbf{1}^\top (\mathbf{A} \circ \mathbf{F}^{lc}(\mathbf{u}^L, \mathbf{u}^R)) \mathbf{w}^R = (\boldsymbol{\psi}^L)^\top \bar{\mathbf{A}} \bar{\mathbf{1}} - \bar{\mathbf{1}}^\top \bar{\mathbf{A}} \boldsymbol{\psi}^R. \quad (\text{A41})$$

Proof. The proof is given in [61] (see also Ref. [48] Lemmas 2 and 3). \square

We can finally prove Theorem 3. To begin, since \mathbf{P}_J^g is diagonal we obtain

$$2(\mathbf{w}^g)^\top \mathbf{P}_J^g \mathbf{Q}_{x_l}^{s,g} \circ \mathbf{F}^{lc}(\mathbf{u}^g, \mathbf{u}^g) \mathbf{1} = 2(\mathbf{w}^g)^\top \mathbf{Q}_{x_l}^{s,g} \circ \mathbf{F}^{lc}(\mathbf{u}^g, \mathbf{u}^g) \mathbf{1}. \quad (\text{A42})$$

Next splitting the right-hand side of (A42) into two terms, taking the transpose of the second term and using the symmetry of the matrix $\mathbf{F}^{lc}(\mathbf{u}^g, \mathbf{u}^g)$, we obtain

$$(\mathbf{w}^g)^\top \mathbf{P}_J^g \mathbf{D}_{x_l}^{s,g} \circ \mathbf{F}^{lc}(\mathbf{u}^g, \mathbf{u}^g) \mathbf{1} = (\mathbf{w}^g)^\top \mathbf{Q}_{x_l}^{s,g} \circ \mathbf{F}^{lc}(\mathbf{u}^g, \mathbf{u}^g) \mathbf{1} + \mathbf{1}^\top (\mathbf{Q}_{x_l}^{s,g})^\top \circ \mathbf{F}^{lc}(\mathbf{u}^g, \mathbf{u}^g) \mathbf{w}^g. \quad (\text{A43})$$

Using the SBP property, $\mathbf{Q}_{x_l}^{s,g} = -(\mathbf{Q}_{x_l}^{s,g})^\top + \mathbf{E}_{x_l}^g$, yields

$$2(\mathbf{w}^g)^\top \mathbf{P}_J^g \mathbf{Q}_{x_l}^{s,g} \circ \mathbf{F}^{lc}(\mathbf{u}^g, \mathbf{u}^g) \mathbf{1} = (\mathbf{w}^g)^\top \mathbf{Q}_{x_l}^{s,g} \circ \mathbf{F}^{lc}(\mathbf{u}^g, \mathbf{u}^g) \mathbf{1} - \mathbf{1}^\top \mathbf{Q}_{x_l}^{s,g} \circ \mathbf{F}^{lc}(\mathbf{u}^g, \mathbf{u}^g) \mathbf{w}^g + \mathbf{1}^\top \mathbf{E}_{x_l}^g \circ \mathbf{F}^{lc}(\mathbf{u}^g, \mathbf{u}^g) \mathbf{w}^g. \quad (\text{A44})$$

Applying Theorem 9 to the first two terms on the right-hand side of (A44) leads to

$$2(\mathbf{w}^g)^\top \mathbf{P}_J^g \mathbf{Q}_{x_l}^{s,g} \circ \mathbf{F}^{lc}(\mathbf{u}^g, \mathbf{u}^g) \mathbf{1} = (\boldsymbol{\psi}^g)^\top \bar{\mathbf{Q}}_{x_l}^{s,g} \bar{\mathbf{1}} - \bar{\mathbf{1}}^\top \bar{\mathbf{Q}}_{x_l}^{s,g} \boldsymbol{\psi}^g + \mathbf{1}^\top \mathbf{E}_{x_l}^g \circ \mathbf{F}^{lc}(\mathbf{u}^g, \mathbf{u}^g) \mathbf{w}^g. \quad (\text{A45})$$

If (A39) holds, then, $\bar{\mathbf{Q}}_{x_l}^{s,g} \bar{\mathbf{1}} = \mathbf{0}$. Furthermore, by a similar reasoning we have

$$\bar{\mathbf{1}}^\top \bar{\mathbf{Q}}_{x_l}^{s,g} = \bar{\mathbf{1}}^\top \left(-(\bar{\mathbf{Q}}_{x_l}^{s,g})^\top + \bar{\mathbf{E}}_{x_l}^g \right) = \bar{\mathbf{1}}^\top \bar{\mathbf{E}}_{x_l}^g.$$

Thus, Equation (A45) reduces to

$$2(\mathbf{w}^g)^\top \mathbf{P}_J^g \mathbf{Q}_{x_l}^{s,g} \circ \mathbf{F}^{lc}(\mathbf{u}^g, \mathbf{u}^g) \mathbf{1} = \mathbf{1}^\top \mathbf{E}_{x_l}^g \circ \mathbf{F}^{lc}(\mathbf{u}^g, \mathbf{u}^g) \mathbf{w}^g - \bar{\mathbf{1}}^\top \bar{\mathbf{E}}_{x_l}^g \boldsymbol{\psi}^g. \quad (\text{A46})$$

The right-hand side of Equation (A46) contains only boundary terms arising from the convective term of the PDE system. For the particular class of SBP operators, we are examining, $E_{x_l}^g$ is diagonal and has nonzeros associated with boundary nodes. Moreover, since $F^{lc}(\mathbf{u}^g, \mathbf{u}^g) \mathbf{w}^g$ is consistent, the block diagonals associated with boundary nodes are simply the diagonal matrix $[F^{(c)}]$.

Appendix B Curvilinear element-wise discretization

The discretization on the element with index k is given as

$$[J^k] \frac{d\mathbf{u}^k}{dt} = \mathbf{r}^k - \sum_{l,m=1}^{dim} \left(D_{\xi_m} \left[J \frac{\partial \xi_m}{\partial x_l} \right]_k + \left[J \frac{\partial \xi_m}{\partial x_l} \right]_k D_{\xi_m} \right) \circ F^{lc}(\mathbf{u}^k, \mathbf{u}^k) \mathbf{1} + \sum_{i,j=1}^{dim} D_{\xi_i} [\tilde{\mathbf{C}}_{i,j}]_k \Theta_j^k + \mathbf{SAT}^{(c)} + \mathbf{SAT}^{(d)} + \mathbf{SAT}^{(bc)} + \mathbf{diss}^{(c)} + \mathbf{diss}^{(d)}, \quad (\text{B47})$$

where

$$[\tilde{\mathbf{C}}_{i,j}]_k \equiv \sum_{l,m=1}^{dim} \left[J \frac{\partial \xi_i}{\partial x_l} \right]_k [\hat{\mathbf{C}}_{l,m}^k] [J^k]^{-1} \left[J \frac{\partial \xi_i}{\partial x_l} \right]_k. \quad (\text{B48})$$

Moreover, Θ_j^k is defined as

$$\Theta_j^k = D_{\xi_j} \mathbf{w}^k + \mathbf{SAT}^{(w)}. \quad (\text{B49})$$

The interface dissipation terms, $\mathbf{diss}^{(c)}$ and $\mathbf{diss}^{(d)}$, are discussed in Appendix C. Below, we describe the remaining SAT terms, where the SATs are constructed for the surface perpendicular to ξ_1 and located where ξ_1 is at a maximum. The $\mathbf{SAT}^{(c)}$ is defined as

$$\mathbf{SAT}^{(c)} \equiv \mathbf{P}^{-1} \sum_{m=1}^{dim} \left\{ \left(\left(\mathbf{R}_{\xi_1}^{(N_{1d})} \right)^T \mathbf{P}_{\xi_1}^\perp \mathbf{R}_{\xi_1}^{(N_{1d})} \left[J \frac{\partial \xi_1}{\partial x_m} \right]_k \right) \circ F^{lc}(\mathbf{u}^k, \mathbf{u}^k) \mathbf{1} - \left(\left(\mathbf{R}_{\xi_1}^{(N_{1d})} \right)^T \mathbf{P}_{\xi_1}^\perp \mathbf{R}_{\xi_{N_{1d}}}^{(1)} \left[J \frac{\partial \xi_1}{\partial x_m} \right]_a \right) \circ F^{lc}(\mathbf{u}^k, \mathbf{u}^a) \mathbf{1} \right\},$$

where \mathbf{u}^a and $\left[J \frac{\partial \xi_1}{\partial x_m} \right]_a$ are the solution and the metrics terms of the adjoining element, respectively.

The $\mathbf{SAT}^{(d)}$ term reads

$$\mathbf{SAT}^{(d)} \equiv -\frac{1}{2} \mathbf{P}^{-1} \sum_{j=1}^{dim} \left(\left(\mathbf{R}_{\xi_1}^{(N_{1d})} \right)^T \mathbf{P}_{\xi_1}^\perp \mathbf{R}_{\xi_1}^{(N_{1d})} [\tilde{\mathbf{C}}_{1,j}]_k \Theta_j^k \mathbf{1} - \left(\mathbf{R}_{\xi_1}^{(N_{1d})} \right)^T \mathbf{P}_{\xi_1}^\perp \mathbf{R}_{\xi_{N_{1d}}}^{(1)} [\tilde{\mathbf{C}}_{1,j}]_a \Theta_j^a \right),$$

where Θ_j^a and $[\tilde{\mathbf{C}}_{1,j}]_a$ are from the adjoining element.

Finally, $\mathbf{SAT}^{(w)}$ indicates the SAT term applied to the gradient of the discrete entropy variables. For example, the $\mathbf{SAT}^{(w)}$ for Θ_1^k is constructed as

$$\mathbf{SAT}^{(w)} \equiv -\frac{1}{2} \mathbf{P}^{-1} \left(\mathbf{R}_{\xi_1}^{(N_{1d})} \right)^T \mathbf{P}_{\xi_1}^\perp \left(\mathbf{R}_{\xi_1}^{(N_{1d})} \mathbf{w}^k - \mathbf{R}_{\xi_1}^{(1)} \mathbf{w}^a \right), \quad (\text{B50})$$

where \mathbf{w}^a is from the adjoining element.

Appendix C Interface dissipation

The $\mathbf{diss}^{(d)}$ term adds interface dissipation for the viscous terms and is constructed as

$$\mathbf{diss}^{(d)} \equiv -\mathbf{P}^{-1} \left(\mathbf{R}_{\xi_1}^{(N_{1d})} \right)^T \mathbf{P}_{\xi_1}^\perp \widetilde{\mathbf{Co}} \left(\mathbf{R}_{\xi_1}^{(N_{1d})} \mathbf{w}^k - \mathbf{R}_{\xi_1}^{(1)} \mathbf{w}^a \right), \quad (\text{C51})$$

where $\widetilde{\mathbf{Co}}$ is an appropriate combination of interface values of $[\tilde{\mathbf{C}}_{1,j}]_k$ and $[\tilde{\mathbf{C}}_{1,j}]_a$ (for example the average) and the terms \mathbf{w}^a and $[\tilde{\mathbf{C}}_{1,j}]_a$ originate from the adjoining element.

We continue to use the same interface for the analysis as in the previous sections. The $\mathbf{diss}^{(d)}$ term from the L element results in

$$\mathbf{diss}^{(d),L} \equiv -(\mathbf{w}^L)^\top \left(\mathbf{R}_{\xi_1}^{(N_{1d})} \right)^\top \mathbf{P}_{\xi_1}^\perp \widetilde{\mathbf{C}}_0 \left(\mathbf{R}_{\xi_1}^{(N_{1d})} \mathbf{w}^L - \mathbf{R}_{\xi_1}^{(1)} \mathbf{w}^R \right), \quad (\text{C52})$$

while for the R element we obtain

$$\mathbf{diss}^{(d),R} \equiv -(\mathbf{w}^R)^\top \left(\mathbf{R}_{\xi_1}^{(1)} \right)^\top \mathbf{P}_{\xi_1}^\perp \widetilde{\mathbf{C}}_0 \left(\mathbf{R}_{\xi_1}^{(1)} \mathbf{w}^R - \mathbf{R}_{\xi_1}^{(N_{1d})} \mathbf{w}^L \right). \quad (\text{C53})$$

Summing (C52) and (C53) gives

$$\mathbf{diss}^{(d),L} + \mathbf{diss}^{(d),R} = -\left(\mathbf{R}_{\xi_1}^{(N_{1d})} \mathbf{w}^L - \mathbf{R}_{\xi_1}^{(1)} \mathbf{w}^R \right)^\top \mathbf{P}_{\xi_1}^\perp \widetilde{\mathbf{C}}_0 \left(\mathbf{R}_{\xi_1}^{(N_{1d})} \mathbf{w}^L - \mathbf{R}_{\xi_1}^{(1)} \mathbf{w}^R \right),$$

which is a negative semi-definite term and therefore does not impact the Lyapunov consistency and stability statement.

Also the Lyapunov consistent SATs terms, $\mathbf{SAT}^{(c)}$, are augmented with dissipative terms inspired by the upwinding used in the Roe approximate Riemann solver, which has the following generic form:

$$\mathbf{F}^* = \frac{\mathbf{F}^+ + \mathbf{F}^-}{2} - \frac{1}{2} \mathbf{Y} |\Lambda| \mathbf{Y}^{-1} (\mathbf{U}^+ - \mathbf{U}^-) \quad (\text{C54})$$

where the superscript “+” denotes quantities evaluated on the side of an interface in the positive direction of the unit normal, and the superscript “-” denotes quantities in the negative direction. Since the Roe flux is not entropy consistent, the central flux in (C54) (i.e., the first term on the right-hand side) is replaced by the numerical fluxes given in the above Lyapunov conservative $\mathbf{SAT}^{(c)}$ terms. To provide entropy dissipation at element interfaces, the dissipative term, i.e., the second term on the right-hand side of (C54) also has to be modified. The approach is constructing a dissipation term that enables Lyapunov stability while remaining accurate and conservative in design order. This last step is accomplished by using the flux Jacobian with respect to the Lyapunov variables rather than the conservative variables [12, 51]. The eigenvectors of the conservative variable flux Jacobian can be scaled such that [64],

$$\frac{\partial \mathbf{U}}{\partial \mathbf{W}} = \mathbf{Y} \mathbf{Y}^\top.$$

Using this approach, after some algebraic manipulation and including the metric terms for curvilinear grids, we arrive at the following expression for the $\mathbf{diss}^{(c)}$,

$$\mathbf{diss}^{(c)} \equiv -\frac{1}{2} \mathbf{P}^{-1} \left(\mathbf{R}_{\xi_1}^{(N_{1d})} \right)^\top \mathbf{P}_{\xi_1}^\perp \left[\left[\frac{\partial \tilde{\mathbf{U}}_1}{\partial \mathbf{W}} \right] \right] \left(\mathbf{R}_{\xi_1}^{(N_{1d})} \mathbf{w}^k - \mathbf{R}_{\xi_1}^{(1)} \mathbf{w}^a \right),$$

where $\left[\left[\frac{\partial \tilde{\mathbf{U}}_1}{\partial \mathbf{W}} \right] \right]$ is a block diagonal matrix constructed from an appropriate average of

$$\frac{\partial \tilde{\mathbf{U}}_m}{\partial \mathbf{W}} \equiv \sum_{l=1}^{dim} J \frac{\partial \xi_m}{\partial x_m} \frac{\partial \mathbf{U}}{\partial \mathbf{W}},$$

from element k and the adjacent element denoted by a . We highlight that, the same approach can be used for dynamic, unstructured grids. We refer the reader to the detailed and clear analysis reported by Yamaleev and co-authors [62].

Now, we compute the resulting term of $\mathbf{diss}^{(c)}$ for an interface shared by two elements denoted by the usual superscripts “ L ” and “ R ”. The contribution from the element L is given by

$$\mathbf{diss}^{(c),L} \equiv -\mathbf{w}^L \left(\mathbf{R}_{\xi_1}^{(N_{1d})} \right)^\top \mathbf{P}_{\xi_1}^\perp \left[\left[\frac{\partial \tilde{\mathbf{U}}_1}{\partial \mathbf{W}} \right] \right] \left(\mathbf{R}_{\xi_1}^{(N_{1d})} \mathbf{w}^L - \mathbf{R}_{\xi_1}^{(1)} \mathbf{w}^R \right), \quad (\text{C55})$$

while for the R element the contribution is

$$diss^{(c),R} \equiv -\mathbf{w}^R \left(\mathbf{R}_{\xi_1}^{(1)} \right)^T \mathbf{P}_{\xi_1}^\perp \left[\left[\frac{\partial \tilde{\mathbf{U}}_1}{\partial \mathbf{W}} \right] \right] \left(\mathbf{R}_{\xi_1}^{(1)} \mathbf{w}^R - \mathbf{R}_{\xi_1}^{(N_{1d})} \mathbf{w}^L \right). \quad (\text{C56})$$

Adding (D71) to (D72) gives

$$diss^{(c),L} + diss^{(c),R} = - \left(\mathbf{R}_{\xi_1}^{(N_{1d})} \mathbf{w}^L - \mathbf{R}_{\xi_1}^{(1)} \mathbf{w}^R \right)^T \mathbf{P}_{\xi_1}^\perp \left[\left[\frac{\partial \tilde{\mathbf{U}}_1}{\partial \mathbf{W}} \right] \right] \left(\mathbf{R}_{\xi_1}^{(N_{1d})} \mathbf{w}^L - \mathbf{R}_{\xi_1}^{(1)} \mathbf{w}^R \right).$$

Appendix D Semi-discrete stability analysis: convective terms

The element-wise Lyapunov consistency (stability) analysis of the diffusive and reaction terms is reported in [8], and it is decoupled from the analysis of the convective term. Thus, in this appendix, we need only to show that the addition of the convective term preserves the Lyapunov consistency of the fully discrete algorithms for reaction-diffusion PDE systems presented in [8]. That is, for the generic element with index k , we need to prove that

$$\begin{aligned} C \equiv & - (\mathbf{w}^k)^T \mathbf{P} \sum_{i,l=1}^{dim} \left(\mathbf{D}_{\xi_i} \left[J \frac{\partial \xi_i}{\partial x_l} \right]_k + \left[J \frac{\partial \xi_i}{\partial x_l} \right]_k \mathbf{D}_{\xi_i} \right) \circ \mathbf{F}^{lc} (\mathbf{u}^k, \mathbf{u}^k) \mathbf{1} \\ & + (\mathbf{w}^k)^T \mathbf{P} \left(\mathbf{SAT}^{(c)} + \mathbf{SAT}^{(bc)} \right) \leq 0. \end{aligned} \quad (\text{D57})$$

As before, we will first drop the boundary condition SAT terms, $\mathbf{SAT}^{(bc)}$, as well as the interface dissipation in the $\mathbf{SAT}^{(c)}$, i.e., the dissipation term $diss^{(c)}$, presented in the previous section. Thus, after using the definition $\mathbf{D}_{\xi_i} = \mathbf{P}^{-1} \mathbf{Q}_{\xi_i}$, Equation (D57) reduces to

$$\begin{aligned} C = & - (\mathbf{w}^k)^T \sum_{i,l=1}^{dim} \left(\mathbf{Q}_{\xi_i} \left[J \frac{\partial \xi_i}{\partial x_l} \right]_k + \left[J \frac{\partial \xi_i}{\partial x_l} \right]_k \mathbf{Q}_{\xi_i} \right) \circ \mathbf{F}^{lc} (\mathbf{u}^k, \mathbf{u}^k) \mathbf{1} \\ & + (\mathbf{w}^k)^T \mathbf{P} \mathbf{SAT}^{(c)}. \end{aligned} \quad (\text{D58})$$

Taking the transpose of the second set of terms on the right-hand side of (D58) (first line), using the SBP property $\mathbf{Q}_{\xi_i}^T = -\mathbf{Q}_{\xi_i} + \mathbf{E}_{\xi_i}$, and the symmetry of $\mathbf{F}^{lc} (\mathbf{u}, \mathbf{u})$, we obtain

$$\begin{aligned} C = & - \sum_{i,l=1}^{dim} \left((\mathbf{w}^k)^T \left(\mathbf{Q}_{\xi_i} \left[J \frac{\partial \xi_i}{\partial x_l} \right]_k \right) \circ \mathbf{F}^{lc} (\mathbf{u}^k, \mathbf{u}^k) \mathbf{1} - \mathbf{1}^T \left(\mathbf{Q}_{\xi_i} \left[J \frac{\partial \xi_i}{\partial x_l} \right]_k \right) \circ \mathbf{F}^{lc} (\mathbf{u}^k, \mathbf{u}^k) \mathbf{w}^k \right) \\ & + \sum_{i,l=1}^{dim} (\mathbf{w}^k)^T \left(\mathbf{E}_{\xi_i} \left[J \frac{\partial \xi_i}{\partial x_l} \right]_k \right) \circ \mathbf{F}^{lc} (\mathbf{u}^k, \mathbf{u}^k) \mathbf{1} + (\mathbf{w}^k)^T \mathbf{P} \mathbf{SAT}^{(c)}. \end{aligned} \quad (\text{D59})$$

Using Theorem 9 on the first sum on the right-hand side of (D59) gives

$$\begin{aligned} C = & - \sum_{i,l=1}^{dim} \left((\boldsymbol{\psi}^k)^T \overline{\mathbf{Q}_{\xi_i}} \left[J \frac{\partial \xi_i}{\partial x_l} \right]_k \overline{\mathbf{1}} - \overline{\mathbf{1}}^T \overline{\mathbf{Q}_{\xi_i}} \left[J \frac{\partial \xi_i}{\partial x_l} \right]_k \boldsymbol{\psi}^k \right) \\ & - \sum_{i,l=1}^{dim} (\mathbf{w}^k)^T \left(\mathbf{E}_{\xi_i} \left[J \frac{\partial \xi_i}{\partial x_l} \right]_k \right) \circ \mathbf{F}^{lc} (\mathbf{u}^k, \mathbf{u}^k) \mathbf{1} + (\mathbf{w}^k)^T \mathbf{P} \mathbf{SAT}^{(c)}. \end{aligned} \quad (\text{D60})$$

The first term on the right-hand side of (D60) is zero via the discrete metric identities assumption (A39), i.e.,

$$\begin{aligned} \sum_{i,l=1}^{dim} (\boldsymbol{\psi}^k)^T \bar{\mathbf{Q}}_{\xi_i} \left[J \frac{\partial \xi_i}{\partial x_l} \right]_k \bar{\mathbf{1}} &= \sum_{i=1}^{dim} (\boldsymbol{\psi}^k)^T \sum_{i=1}^{dim} \bar{\mathbf{Q}}_{\xi_i} \left[J \frac{\partial \xi_i}{\partial x_l} \right]_k \bar{\mathbf{1}} \\ &= \sum_{i=1}^{dim} (\boldsymbol{\psi}^k)^T \mathbf{P} \sum_{i=1}^{dim} \bar{\mathbf{D}}_{\xi_i} \left[J \frac{\partial \xi_i}{\partial x_l} \right]_k \bar{\mathbf{1}} = 0. \end{aligned}$$

Thus, Equation (D60) reduces to

$$C = \sum_{i,l=1}^{dim} \bar{\mathbf{1}}^T \bar{\mathbf{Q}}_{\xi_i} \left[J \frac{\partial \xi_i}{\partial x_l} \right]_k \boldsymbol{\psi}^k - \sum_{i,l=1}^{dim} (\mathbf{w}^k)^T \left(\mathbf{E}_{\xi_i} \left[J \frac{\partial \xi_i}{\partial x_l} \right]_k \right) \circ \mathbf{F}^{lc} (\mathbf{u}^k, \mathbf{u}^k) \mathbf{1} + (\mathbf{w}^k)^T \mathbf{P} \mathbf{S} \mathbf{A} \mathbf{T}^{(c)}. \quad (\text{D61})$$

Finally, using consistency of the SBP operator (i.e., $\mathbf{D}_{\xi_i} \mathbf{1} = 0 \rightarrow \mathbf{1}^T \mathbf{Q}_{\xi_i} = \mathbf{1}^T \mathbf{E}_{\xi_i}$), Equation (D61) reduces to

$$C = \sum_{i,l=1}^{dim} \bar{\mathbf{1}}^T \bar{\mathbf{E}}_{\xi_i} \left[J \frac{\partial \xi_i}{\partial x_l} \right]_k \boldsymbol{\psi}^k - \sum_{i,l=1}^{dim} (\mathbf{w}^k)^T \left(\mathbf{E}_{\xi_i} \left[J \frac{\partial \xi_i}{\partial x_l} \right]_k \right) \circ \mathbf{F}^{lc} (\mathbf{u}^k, \mathbf{u}^k) \mathbf{1} + (\mathbf{w}^k)^T \mathbf{P} \mathbf{S} \mathbf{A} \mathbf{T}^{(c)}. \quad (\text{D62})$$

All the terms in (D62) are surface terms. We continue the analysis by considering the contributions at a particular surface. For the L element, the surface terms are

$$\begin{aligned} C_L &\equiv \sum_{l=1}^{dim} \bar{\mathbf{1}}^T \left(\bar{\mathbf{R}}_{\xi_1}^{(N_{1d})} \right)^T \bar{\mathbf{P}}_{\xi_1}^\perp \bar{\mathbf{R}}_{\xi_1}^{(N_{1d})} \boldsymbol{\psi}^L \\ &\quad - \sum_{l=1}^{dim} (\mathbf{w}^L)^T \left(\left(\mathbf{R}_{\xi_1}^{(N_{1d})} \right)^T \mathbf{P}_{\xi_1}^\perp \mathbf{R}_{\xi_1}^{(N_{1d})} \left[J \frac{\partial \xi_i}{\partial x_l} \right]_L \right) \circ \mathbf{F}^{lc} (\mathbf{u}^L, \mathbf{u}^L) \mathbf{1} \\ &\quad + \sum_{l=1}^{dim} (\mathbf{w}^L)^T \left(\left(\mathbf{R}_{\xi_1}^{(N_{1d})} \right)^T \mathbf{P}_{\xi_1}^\perp \mathbf{R}_{\xi_1}^{(N_{1d})} \left[J \frac{\partial \xi_i}{\partial x_l} \right]_L \right) \circ \mathbf{F}^{lc} (\mathbf{u}^L, \mathbf{u}^L) \mathbf{1} \\ &\quad - \sum_{l=1}^{dim} (\mathbf{w}^L)^T \left(\left(\mathbf{R}_{\xi_1}^{(N_{1d})} \right)^T \mathbf{P}_{\xi_1}^\perp \mathbf{R}_{\xi_1}^{(1)} \left[J \frac{\partial \xi_i}{\partial x_l} \right]_R \right) \circ \mathbf{F}^{lc} (\mathbf{u}^L, \mathbf{u}^R) \mathbf{1}. \end{aligned} \quad (\text{D63})$$

Thus, C_L reduces to

$$\begin{aligned} C_L &\equiv \sum_{l=1}^{dim} \bar{\mathbf{1}}^T \left(\bar{\mathbf{R}}_{\xi_1}^{(N_{1d})} \right)^T \bar{\mathbf{P}}_{\xi_1}^\perp \bar{\mathbf{R}}_{\xi_1}^{(N_{1d})} \boldsymbol{\psi}^L \\ &\quad - \sum_{l=1}^{dim} (\mathbf{w}^L)^T \left(\left(\mathbf{R}_{\xi_1}^{(N_{1d})} \right)^T \mathbf{P}_{\xi_1}^\perp \mathbf{R}_{\xi_1}^{(1)} \left[J \frac{\partial \xi_i}{\partial x_l} \right]_R \right) \circ \mathbf{F}^{lc} (\mathbf{u}^L, \mathbf{u}^R) \mathbf{1}. \end{aligned} \quad (\text{D64})$$

An identical analysis for the contributions from the R element results in

$$\begin{aligned} C_R &\equiv - \sum_{l=1}^{dim} \bar{\mathbf{1}}^T \left(\bar{\mathbf{R}}_{\xi_1}^{(1)} \right)^T \bar{\mathbf{P}}_{\xi_1}^\perp \bar{\mathbf{R}}_{\xi_1}^{(1)} \boldsymbol{\psi}^R \\ &\quad + \sum_{l=1}^{dim} (\mathbf{w}^R)^T \left(\left(\mathbf{R}_{\xi_1}^{(1)} \right)^T \mathbf{P}_{\xi_1}^\perp \mathbf{R}_{\xi_1}^{(N_{1d})} \left[J \frac{\partial \xi_i}{\partial x_l} \right]_L \right) \circ \mathbf{F}^{lc} (\mathbf{u}^R, \mathbf{u}^L) \mathbf{1}. \end{aligned} \quad (\text{D65})$$

Suming (D64) and (D65) yields

$$\begin{aligned}
C_L + C_R &= \sum_{l=1}^{dim} \bar{\mathbf{I}}^T \left(\bar{\mathbf{R}}_{\xi_1}^{(N_{1d})} \right)^T \bar{\mathbf{P}}_{\xi_1}^\perp \bar{\mathbf{R}}_{\xi_1}^{(N_{1d})} \boldsymbol{\psi}^L - \sum_{l=1}^{dim} \bar{\mathbf{I}}^T \left(\bar{\mathbf{R}}_{\xi_1}^{(1)} \right)^T \bar{\mathbf{P}}_{\xi_1}^\perp \bar{\mathbf{R}}_{\xi_1}^{(1)} \boldsymbol{\psi}^R \\
&\quad - \sum_{l=1}^{dim} (\boldsymbol{w}^L)^T \left(\left(\mathbf{R}_{\xi_1}^{(N_{1d})} \right)^T \mathbf{P}_{\xi_1}^\perp \mathbf{R}_{\xi_1}^{(1)} \left[J \frac{\partial \xi_i}{\partial x_l} \right]_R \right) \circ \mathbf{F}^{lc}(\boldsymbol{u}^L, \boldsymbol{u}^R) \mathbf{1} \\
&\quad + \sum_{l=1}^{dim} (\boldsymbol{w}^R)^T \left(\left(\mathbf{R}_{\xi_1}^{(1)} \right)^T \mathbf{P}_{\xi_1}^\perp \mathbf{R}_{\xi_1}^{(N_{1d})} \left[J \frac{\partial \xi_i}{\partial x_l} \right]_L \right) \circ \mathbf{F}^{lc}(\boldsymbol{u}^R, \boldsymbol{u}^L) \mathbf{1}.
\end{aligned} \tag{D66}$$

Taking the transpose of the terms in the last sum on the right-hand side of (D66) and using the symmetry of $\mathbf{F}^{lc}(\boldsymbol{u}, \boldsymbol{u})$ (i.e., $\mathbf{F}^{lc}(\boldsymbol{u}^L, \boldsymbol{u}^R) = \mathbf{F}^{lc}(\boldsymbol{u}^R, \boldsymbol{u}^L)^T$), Equation (D66) reduces to

$$\begin{aligned}
C_L + C_R &= \sum_{l=1}^{dim} \bar{\mathbf{I}}^T \left(\bar{\mathbf{R}}_{\xi_1}^{(N_{1d})} \right)^T \bar{\mathbf{P}}_{\xi_1}^\perp \bar{\mathbf{R}}_{\xi_1}^{(N_{1d})} \boldsymbol{\psi}^L - \sum_{l=1}^{dim} \bar{\mathbf{I}}^T \left(\bar{\mathbf{R}}_{\xi_1}^{(1)} \right)^T \bar{\mathbf{P}}_{\xi_1}^\perp \bar{\mathbf{R}}_{\xi_1}^{(1)} \boldsymbol{\psi}^R \\
&\quad - \sum_{l=1}^{dim} (\boldsymbol{w}^L)^T \left(\left(\mathbf{R}_{\xi_1}^{(N_{1d})} \right)^T \mathbf{P}_{\xi_1}^\perp \mathbf{R}_{\xi_1}^{(1)} \left[J \frac{\partial \xi_i}{\partial x_l} \right]_R \right) \circ \mathbf{F}^{lc}(\boldsymbol{u}^L, \boldsymbol{u}^R) \mathbf{1} \\
&\quad + \sum_{l=1}^{dim} \mathbf{1}^T \left(\left[J \frac{\partial \xi_i}{\partial x_l} \right]_L \left(\mathbf{R}_{\xi_1}^{(N_{1d})} \right)^T \mathbf{P}_{\xi_1}^\perp \mathbf{R}_{\xi_1}^{(N_{1d})} \right) \circ \mathbf{F}^{lc}(\boldsymbol{u}^L, \boldsymbol{u}^R) (\boldsymbol{w}^R)^T.
\end{aligned} \tag{D67}$$

Now, considering that $\left(\mathbf{R}_{\xi_1}^{(N_{1d})} \right)^T \mathbf{P}_{\xi_1}^\perp \mathbf{R}_{\xi_1}^{(1)} \left[J \frac{\partial \xi_i}{\partial x_l} \right]_R$ is diagonal and picks off the values of the metrics at the surface nodes and that at the surface nodes the metrics are the same, we have

$$\left[J \frac{\partial \xi_i}{\partial x_l} \right]_L \left(\mathbf{R}_{\xi_1}^{(N_{1d})} \right)^T \mathbf{P}_{\xi_1}^\perp \mathbf{R}_{\xi_1}^{(N_{1d})} = \left(\mathbf{R}_{\xi_1}^{(N_{1d})} \right)^T \mathbf{P}_{\xi_1}^\perp \mathbf{R}_{\xi_1}^{(1)} \left[J \frac{\partial \xi_i}{\partial x_l} \right]_R. \tag{D68}$$

Using identity (D68), Equation (D67) becomes

$$\begin{aligned}
C_L + C_R &= \sum_{l=1}^{dim} \bar{\mathbf{I}}^T \left(\bar{\mathbf{R}}_{\xi_1}^{(N_{1d})} \right)^T \bar{\mathbf{P}}_{\xi_1}^\perp \bar{\mathbf{R}}_{\xi_1}^{(N_{1d})} \boldsymbol{\psi}^L - \sum_{l=1}^{dim} \bar{\mathbf{I}}^T \left(\bar{\mathbf{R}}_{\xi_1}^{(1)} \right)^T \bar{\mathbf{P}}_{\xi_1}^\perp \bar{\mathbf{R}}_{\xi_1}^{(1)} \boldsymbol{\psi}^R \\
&\quad - \sum_{l=1}^{dim} (\boldsymbol{w}^L)^T \left(\left(\mathbf{R}_{\xi_1}^{(N_{1d})} \right)^T \mathbf{P}_{\xi_1}^\perp \mathbf{R}_{\xi_1}^{(1)} \left[J \frac{\partial \xi_i}{\partial x_l} \right]_R \right) \circ \mathbf{F}^{lc}(\boldsymbol{u}^L, \boldsymbol{u}^R) \mathbf{1} \\
&\quad + \sum_{l=1}^{dim} \mathbf{1}^T \left(\left(\mathbf{R}_{\xi_1}^{(N_{1d})} \right)^T \mathbf{P}_{\xi_1}^\perp \mathbf{R}_{\xi_1}^{(N_{1d})} \left[J \frac{\partial \xi_i}{\partial x_l} \right]_R \right) \circ \mathbf{F}^{lc}(\boldsymbol{u}^L, \boldsymbol{u}^R) (\boldsymbol{w}^R)^T.
\end{aligned} \tag{D69}$$

Now, we apply Theorem 9 on the last two sums on the right-hand side of (D69) which gives

$$\begin{aligned}
C_L + C_R &= \sum_{l=1}^{dim} \bar{\mathbf{I}}^T \left(\bar{\mathbf{R}}_{\xi_1}^{(N_{1d})} \right)^T \bar{\mathbf{P}}_{\xi_1}^\perp \bar{\mathbf{R}}_{\xi_1}^{(N_{1d})} \boldsymbol{\psi}^L - \sum_{l=1}^{dim} \bar{\mathbf{I}}^T \left(\bar{\mathbf{R}}_{\xi_1}^{(1)} \right)^T \bar{\mathbf{P}}_{\xi_1}^\perp \bar{\mathbf{R}}_{\xi_1}^{(1)} \boldsymbol{\psi}^R \\
&\quad - \sum_{l=1}^d (\boldsymbol{\psi}^L)^T \left(\left(\bar{\mathbf{R}}_{\xi_1}^{(N_{1d})} \right)^T \bar{\mathbf{P}}_{\xi_1}^\perp \bar{\mathbf{R}}_{\xi_1}^{(1)} \left[J \frac{\partial \xi_i}{\partial x_l} \right]_R \right) \bar{\mathbf{I}} \\
&\quad + \sum_{l=1}^{dim} \bar{\mathbf{I}}^T \left(\left(\bar{\mathbf{R}}_{\xi_1}^{(N_{1d})} \right)^T \bar{\mathbf{P}}_{\xi_1}^\perp \bar{\mathbf{R}}_{\xi_1}^{(N_{1d})} \left[J \frac{\partial \xi_i}{\partial x_l} \right]_R \right) \boldsymbol{\psi}^R = 0,
\end{aligned} \tag{D70}$$

where the final equality follows from using identity (D68). Thus, the interface terms do not destroy the result generated from the discrete diffusion operator analysis reported in [8].

Next we analyze the effect of the additional dissipation. The contribution from element L is

$$diss^{(c),L} \equiv -\mathbf{w}^L \left(\mathbf{R}_{\xi_1}^{(N_{1d})} \right)^T \mathbf{P}_{\xi_1}^\perp \left[\left[\frac{\partial \tilde{\mathbf{U}}_1}{\partial \mathbf{W}} \right] \right] \left(\mathbf{R}_{\xi_1}^{(N_{1d})} \mathbf{w}^L - \mathbf{R}_{\xi_1}^{(1)} \mathbf{w}^R \right), \quad (\text{D71})$$

while for the R element the contribution is

$$diss^{(c),R} \equiv -\mathbf{w}^R \left(\mathbf{R}_{\xi_1}^{(1)} \right)^T \mathbf{P}_{\xi_1}^\perp \left[\left[\frac{\partial \tilde{\mathbf{U}}_1}{\partial \mathbf{W}} \right] \right] \left(\mathbf{R}_{\xi_1}^{(1)} \mathbf{w}^R - \mathbf{R}_{\xi_1}^{(N_{1d})} \mathbf{w}^L \right). \quad (\text{D72})$$

Adding (D71) to (D72) gives

$$diss^{(c),L} + diss^{(c),R} = - \left(\mathbf{R}_{\xi_1}^{(N_{1d})} \mathbf{w}^L - \mathbf{R}_{\xi_1}^{(1)} \mathbf{w}^R \right)^T \mathbf{P}_{\xi_1}^\perp \left[\left[\frac{\partial \tilde{\mathbf{U}}_1}{\partial \mathbf{W}} \right] \right] \left(\mathbf{R}_{\xi_1}^{(N_{1d})} \mathbf{w}^L - \mathbf{R}_{\xi_1}^{(1)} \mathbf{w}^R \right),$$

which is a negative semi-definite term since $\left[\left[\frac{\partial \tilde{\mathbf{U}}_1}{\partial \mathbf{W}} \right] \right]$ is symmetric positive-semi definite. Therefore, it does not impact the Lyapunov consistency statement.

Appendix E Mesh Convergence Study

To evaluate the impact of mesh refinement on the convergence to the equilibrium point of the proposed algorithms, we conduct numerical simulations of the dimerization model (51) using identical parameter settings, boundary conditions, and initial conditions. The simulations are performed within a cubic domain with a side length of 1 unit, discretized with 8, 16, 32, 64, 128, and 256 quadrilateral cells in each coordinate direction. We determine the time T_{eq} at which the maximum norm of the difference between the numerical solution and the equilibrium value becomes less than or equal to 10^{-8} . The T_{eq} results are presented in Figure E1, plotted against the number of cells, K . As the cell density increases, the solution progressively approaches the equilibrium point. Notably, the reported times for the grids of 128 and 256 cells demonstrate negligible differences and are practically indistinguishable.

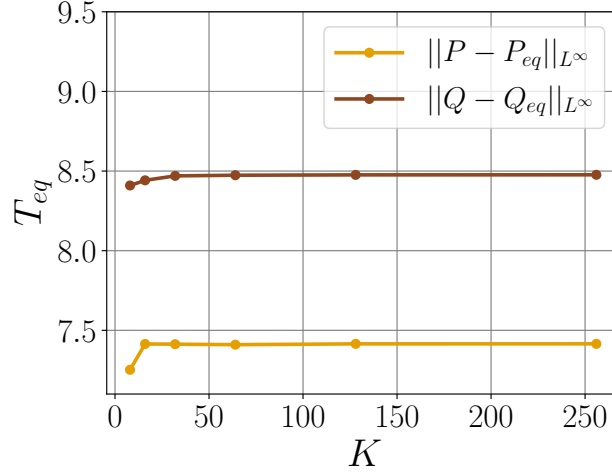


Fig. E1: Effect of the mesh refinement on the convergence to the equilibrium for the dimerization model (51).

Appendix F Discrete Error Norms

In this work, we used the following formula of L^1 , L^2 , L^∞ norms to compute the error:

$$\begin{aligned}\|\mathbf{U}\|_{L^1} &= \Omega_c^{-1} \sum_{j=1}^{N_{el}} \mathbf{1}^T \mathbf{P}_j \mathbf{J}_j \text{abs}(\mathbf{U}_j), \\ \|\mathbf{U}\|_{L^2}^2 &= \Omega_c^{-1} \sum_{j=1}^{N_{el}} \mathbf{U}_j^T \mathbf{P}_j \mathbf{J}_j \mathbf{U}_j, \\ \|\mathbf{U}\|_{L^\infty} &= \max_{j=1 \dots N_{el}} \text{abs}(\mathbf{U}_j),\end{aligned}\tag{F73}$$

where \mathbf{J}_j represents the metric Jacobian of the curvilinear transformation mapping the physical space to the computational space of the j^{th} hexahedral element. The mesh's total number of hexahedral elements is denoted by N_{el} . In addition, Ω_c corresponds to the volume of the domain of interest Ω associated with the considered PDE or system of PDEs. The volume Ω_c is determined as

$$\Omega_c \equiv \sum_{\kappa=1}^K \mathbf{1}_\kappa^T \mathbf{P}^\kappa \mathbf{J}_j \mathbf{1}_\kappa,\tag{F74}$$

where $\mathbf{1}_\kappa$ denotes a vector of ones with a length equivalent to the number of nodes on the κ^{th} element.

Acknowledgments

The work described in this paper was supported by King Abdullah University of Science and Technology through the grant number BAS/1/1663-01-01. The authors are also thankful for the computing resources of the Supercomputing Laboratory at King Abdullah University of Science and Technology.

Declarations

Conflict of interest. The authors declare that they have no conflict of interest.

Availability of code, data, and materials.

References

- [1] Krstic, M., Smyshlyaev, A.: Backstepping boundary control for first-order hyperbolic pdes and application to systems with actuator and sensor delays. *Systems & Control Letters* **57**(9), 750–758 (2008) <https://doi.org/10.1016/j.sysconle.2008.02.005>
- [2] Burton, T.A.: *Stability by Fixed Point Theory for Functional Differential Equations* vol. 1. Courier Corporation, (2013)
- [3] Greenberg, J.M., Ta Tsien, L.: The effect of boundary damping for the quasilinear wave equation. *Journal of Differential Equations* **52**(1), 66–75 (1984) [https://doi.org/10.1016/0022-0396\(84\)90135-9](https://doi.org/10.1016/0022-0396(84)90135-9)
- [4] Komornik, V.: *Exact Controllability and Stabilization: the Multiplier Method* vol. 39. Wiley Chichester, (1994)
- [5] Krstic, M., Guo, B.-Z., Balogh, A., Smyshlyaev, A.: Output-feedback stabilization of an unstable wave equation. *Automatica* **44**(1), 63–74 (2008) <https://doi.org/10.1016/j.automatica.2007.05.012>
- [6] Smyshlyaev, A., Cerpa, E., Krstic, M.: Boundary stabilization of a 1-D wave equation with in-domain antidamping. *SIAM Journal on Control and Optimization* **48**(6), 4014–4031 (2010) <https://doi.org/10.1137/080742646>

- [7] Buonomo, B., Rionero, S.: On the Lyapunov stability for SIR epidemic models with general nonlinear incidence rate. *Applied Mathematics and Computation* **217**(8), 4010–4016 (2010) <https://doi.org/10.1016/j.amc.2010.10.007>
- [8] Al Jahdali, R., Del Rey Fernández, D.C., Dalcin, L., Sayyari, M., Markowich, P., Parsani, M.: Fully discrete Lyapunov consistent discretizations for parabolic reaction-diffusion equations with r species. *Communications on Applied Mathematics and Computation* (2024) <https://doi.org/10.1007/s42967-024-00425-7>
- [9] Tadmor, E.: Entropy stability theory for difference approximations of nonlinear conservation laws and related time-dependent problems. *Acta Numerica* **12**, 451–512 (2003) <https://doi.org/10.1017/S0962492902000156>
- [10] Svärd, M., Nordström, J.: Review of summation-by-parts schemes for initial-boundary-value-problems. *Journal of Computational Physics* **268**(1), 17–38 (2014) <https://doi.org/10.1016/j.jcp.2014.02.031>
- [11] Del Rey Fernández, D.C., Hicken, J.E., Zingg, D.W.: Review of summation-by-parts operators with simultaneous approximation terms for the numerical solution of partial differential equations. *Computers & Fluids* **95**(22), 171–196 (2014) <https://doi.org/10.1016/j.compfluid.2014.02.016>
- [12] Carpenter, M.H., Fisher, T.C., Nielsen, E.J., Frankel, S.H.: Entropy stable spectral collocation schemes for the Navier–Stokes equations: discontinuous interfaces. *SIAM Journal on Scientific Computing* **36**(5), 835–867 (2014) <https://doi.org/10.1137/130932193>
- [13] Parsani, M., Carpenter, M.H., Fisher, T.C., Nielsen, E.J.: Entropy stable staggered grid discontinuous spectral collocation methods of any order for the compressible Navier–Stokes equations. *SIAM Journal on Scientific Computing* **38**(5), 3129–3162 (2016) <https://doi.org/10.1137/15M1043510>
- [14] Carpenter, M.H., Gottlieb, D., Abarbanel, S.: Time-stable boundary conditions for finite-difference schemes solving hyperbolic systems: Methodology and application to high-order compact schemes. *Journal of Computational Physics* **111**(2), 220–236 (1994) <https://doi.org/10.1006/jcph.1994.1057>
- [15] Carpenter, M.H., Nordström, J., Gottlieb, D.: A stable and conservative interface treatment of arbitrary spatial accuracy. *Journal of Computational Physics* **148**(2), 341–365 (1999) <https://doi.org/10.1006/jcph.1998.6114>
- [16] Nordström, J., Carpenter, M.H.: Boundary and interface conditions for high-order finite-difference methods applied to the Euler and Navier–Stokes equations. *Journal of Computational Physics* **148**(2), 621–645 (1999) <https://doi.org/10.1006/jcph.1998.6133>
- [17] Mattsson, K.: Boundary procedures for summation-by-parts operators. *Journal of Scientific Computing* **18**(1), 133–153 (2003) <https://doi.org/10.1023/A:1020342429644>
- [18] Parsani, M., Carpenter, M.H., Nielsen, E.J.: Entropy stable discontinuous interfaces coupling for the three-dimensional compressible Navier–Stokes equations. *Journal of Computational Physics* **290**, 132–138 (2015) <https://doi.org/10.1016/j.jcp.2015.02.042>
- [19] Del Rey Fernández, D.C., Carpenter, M.H., Dalcin, L., Zampini, S., Parsani, M.: Entropy stable h/p -nonconforming discretization with the summation-by-parts property for the compressible Euler and Navier–Stokes equations. *SN Partial Differential Equations and Applications* **1**(2), 1–54 (2020) <https://doi.org/10.1007/s42985-020-00009-z>
- [20] Ketcheson, D.I.: Relaxation Runge–Kutta methods: Conservation and stability for inner-product norms. *SIAM Journal on Numerical Analysis* **57**(6), 2850–2870 (2019) <https://doi.org/10.1137/19M1263662>

- [21] Ranocha, H., Sayyari, M., Dalcin, L., Parsani, M., Ketcheson, D.I.: Relaxation Runge–Kutta methods: Fully-discrete explicit entropy-stable schemes for the Euler and Navier–Stokes equations. Accepted in *SIAM Journal on Scientific Computing* **42**(2), 612–638 (2019) <https://doi.org/10.1137/19M1263480>
- [22] Parsani, M., Boukharfane, R., Nolasco, I.R., Del Rey Fernández, D.C., Zampini, S., Hadri, B., Dalcin, L.: High-order accurate entropy-stable discontinuous collocated galerkin methods with the summation-by-parts property for compressible cfd frameworks: Scalable ssc algorithms and flow solver. *Journal of Computational Physics* **424**, 109844 (2021) <https://doi.org/10.1016/j.jcp.2020.109844>
- [23] LaSalle, J.P., Lefschetz, S.: *Stability by Liapunov’s Direct Method: With Applications. Mathematics in science and engineering: A series of monographs and textbooks.* Academic Press, (1961)
- [24] LaSalle, J.P., Artstein, Z.: *The Stability of Dynamical Systems.* CBMS-NSF Regional Conference Series in Applied Mathematics. Society for Industrial and Applied Mathematics, (1976)
- [25] Harten, A.: On the symmetric form of systems of conservation laws with entropy. *Journal of Computational Physics* **49**(1), 151–164 (1983) [https://doi.org/10.1016/0021-9991\(83\)90118-3](https://doi.org/10.1016/0021-9991(83)90118-3)
- [26] Tadmor, E.: Skew-selfadjoint form for systems of conservation laws. *Journal of Mathematical Analysis and Applications* **103**(2), 428–442 (1984) [https://doi.org/10.1016/0022-247X\(84\)90139-2](https://doi.org/10.1016/0022-247X(84)90139-2)
- [27] Courant, R., Hilbert, D.: *Methods of Mathematical Physics, Volume 1* vol. 1. John Wiley & Sons, (2008)
- [28] Lax, P.D.: *Hyperbolic Systems of Conservation Laws and the Mathematical Theory of Shock Waves.* SIAM, (1973). <https://doi.org/10.1137/1.9781611970562.fm>
- [29] Smoller, J.: *Shock Waves and Reactiondiffusion Equations* vol. 258. Springer, (2012). <https://doi.org/10.1007/978-1-4684-0152-3>
- [30] Whitham, G.B.: *Linear and Nonlinear Waves.* John Wiley & Sons, (2011). <https://doi.org/10.1002/9781118032954>
- [31] Serre, D.: *Systems of Conservation Laws 2: Geometric Structures, Oscillations, and Initial-Boundary Value Problems* vol. 2. Cambridge University Press, (1999)
- [32] Bressan, A.: *Hyperbolic Systems of Conservation Laws: the One-dimensional Cauchy Problem* vol. 20. Oxford University Press, USA, (2000). <https://doi.org/10.1093/oso/9780198507000.001.0001>
- [33] Dafermos, C.M.: *Hyperbolic Conservation Laws in Continuum Physics* vol. 325. Springer, (2016). <https://doi.org/10.1007/978-3-662-49451-6>
- [34] Khalil, H.K.: *Nonlinear Systems; 3rd Ed.* Prentice-Hall, Upper Saddle River, NJ (2002)
- [35] Fisher, T.C., Carpenter, M.H., Nordström, J., Yamaleev, N.K.: Discretely conservative finite-difference formulations for nonlinear conservation laws in split form: Theory and boundary conditions. *Journal of Computational Physics* **234**(1), 353–375 (2013) <https://doi.org/10.1016/j.jcp.2012.09.026>
- [36] Curtain, R., Zwart, H.: *Introduction to Infinite-dimensional Systems Theory: a State-space Approach* vol. 71. Springer, (2020). <https://doi.org/10.1007/978-1-0716-0590-5>
- [37] Luo, Z.-H., Guo, B.-Z., Morgül, Ö.: *Stability and Stabilization of Infinite Dimensional Systems with Applications.* Springer, (1999). <https://doi.org/10.1007/978-1-4471-0419-3>
- [38] Kreiss, H.-O., Scherer, G.: *Finite element and finite difference methods for hyperbolic partial*

- differential equations. In: Boor, C. (ed.) *Mathematical Aspects of Finite Elements in Partial Differential Equations*, pp. 195–212. Academic Press, (1974). <https://doi.org/10.1016/B978-0-12-208350-1.50012-1>
- [39] Gustafsson, B., Kreiss, H.O., Oliger, J.: *Time-Dependent Problems and Difference Methods*. Pure and Applied Mathematics: A Wiley Series of Texts, Monographs and Tracts. Wiley, (2013). <https://doi.org/10.1002/9781118548448>
- [40] Nordström, J., Carpenter, M.H.: High-order finite-difference methods, multidimensional linear problems, and curvilinear coordinates. *Journal of Computational Physics* **173**(1), 149–174 (2001) <https://doi.org/10.1006/jcph.2001.6864>
- [41] Svärd, M., Nordström, J.: A stable high-order finite difference scheme for the compressible Navier–Stokes equations: no-slip wall boundary conditions. *Journal of Computational Physics* **227**(10), 4805–4824 (2008) <https://doi.org/10.1016/j.jcp.2007.12.028>
- [42] Mattsson, K., Ham, F., Iaccarino, G.: Stable boundary treatment for the wave equation on second-order form. *Journal of Scientific Computing* **41**(3), 366–383 (2009) <https://doi.org/10.1007/s10915-009-9305-1>
- [43] Parsani, M., Carpenter, M.H., Nielsen, E.J.: Entropy stable wall boundary conditions for the three-dimensional compressible Navier–Stokes equations. *Journal of Computational Physics* **292**(1), 88–113 (2015) <https://doi.org/10.1016/j.jcp.2015.03.026>
- [44] Del Rey Fernández, D.C., Hicken, J.E., Zingg, D.W.: Simultaneous approximation terms for multidimensional summation-by-parts operators. *Journal of Scientific Computing* **1**(75) (2018) <https://doi.org/10.1007/s10915-017-0523-7>
- [45] Yang, J., Crean, J., Hicken, J.E.: Interior penalties for summation-by-parts discretizations of linear second-order differential equations. *Journal of Scientific Computing* **75**, 1385–1414 (2018) <https://doi.org/10.1007/s10915-017-0591-8>
- [46] Duru, K., Gabriel, A.-A., Kreiss, G.: On energy stable discontinuous Galerkin spectral element approximations of the perfectly matched layer for the wave equation. *Computer Methods in Applied Mechanics and Engineering* **350**, 898–937 (2019) <https://doi.org/10.1016/j.cma.2019.02.036>
- [47] Del Rey Fernández, D.C., Boom, P.D., Carpenter, M.H., Zingg, D.W.: Extension of tensor-product generalized and dense-norm summation-by-parts operators to curvilinear coordinates. accepted in *Journal of Scientific Computing* (2019) <https://doi.org/10.1007/s10915-019-01011-3>
- [48] Crean, J., Hicken, J.E., Del Rey Fernández, D.C., Zingg, D.W., Carpenter, M.H.: Entropy-stable summation-by-parts discretization of the Euler equations on general curved elements. *Journal of Computational Physics* **356**, 410–438 (2018) <https://doi.org/10.1016/j.jcp.2017.12.015>
- [49] Ålund, O., Nordström, J.: Encapsulated high order difference operators on curvilinear non-conforming grids. *Journal of Computational Physics* **385**, 209–224 (2019) <https://doi.org/10.1016/j.jcp.2019.02.007>
- [50] Hicken, J.E., Del Rey Fernández, D.C., Zingg, D.W.: Multidimensional summation-by-part operators: General theory and application to simplex elements. *SIAM Journal on Scientific Computing* **4**(38) (2016) <https://doi.org/10.1137/15M1038360>
- [51] Fisher, T.C., Carpenter, M.H.: High-order entropy stable finite difference schemes for nonlinear conservation laws: Finite domains. *Journal of Computational Physics* **252**(1), 518–557 (2013) <https://doi.org/10.1016/j.jcp.2013.06.014>
- [52] Butcher, J.C.: *Numerical Methods for Ordinary Differential Equations*. John Wiley & Sons Ltd, (2008). <https://doi.org/10.1002/9780470753767>

- [53] Hairer, E., Iserles, A., Sanz-Serna, J.M.: Equilibria of Runge–Kutta methods. *Numerische Mathematik* **58**(1), 243–254 (1990) <https://doi.org/10.1007/BF01385623>
- [54] Griffiths, D., Sweby, P., Yee, H.C.: On spurious asymptotic numerical solutions of explicit Runge–Kutta methods. *IMA Journal of Numerical Analysis* **12**(3), 319–338 (1992) <https://doi.org/10.1093/imanum/12.3.319>
- [55] Iserles, A.: Stability and dynamics of numerical methods for nonlinear ordinary differential equations. *IMA Journal of Numerical Analysis* **10**, 1–30 (1990) <https://doi.org/10.1093/imanum/10.1.1>
- [56] Newell, A.C.: Finite amplitude instabilities of partial difference equations. *SIAM Journal on Applied Mathematics* **33**(1), 133–160 (1977) <https://doi.org/10.1137/0133010>
- [57] Brezzi, F., Ushiki, S., Fujii, H.: Real and ghost bifurcation dynamics in difference schemes for ODEs. In: *Numerical Methods for Bifurcation Problems*, pp. 79–104. Springer, (1984). https://doi.org/10.1007/978-3-0348-6256-1_6
- [58] Shear, D.: An analog of the boltzmann h-theorem (a liapunov function) for systems of coupled chemical reactions. *Journal of theoretical biology* **16**(2), 212–228 (1967) [https://doi.org/10.1016/0022-5193\(67\)90005-7](https://doi.org/10.1016/0022-5193(67)90005-7)
- [59] Roy, C.J.: Review of code and solution verification procedures for computational simulation. *Journal of Computational Physics* **205**(1), 131–156 (2005) <https://doi.org/10.1016/j.jcp.2004.10.036>
- [60] Al Jahdali, R., Dalcin, L., Parsani, M.: On the performance of relaxation and adaptive explicit rungekutta schemes for high-order compressible flow simulations. *Journal of Computational Physics* **464**, 111333 (2022) <https://doi.org/10.1016/j.jcp.2022.111333>
- [61] Fernandez, D.D.R., Carpenter, M.H., Dalcin, L., Fredrich, L., Rojas, D., Winters, A., Gassner, G., Zampini, S., Parsani, M.: Entropy stable nonconforming discretizations with the summation-by-parts property for curvilinear coordinates. NASA/TM20220574 (2020)
- [62] Yamaleev, N.K., Fernandez, D.C.D.R., Lou, J., Carpenter, M.H.: Entropy stable spectral collocation schemes for the 3-D navier-stokes equations on dynamic unstructured grids. *Journal of Computational Physics* **399**, 108897 (2019) <https://doi.org/10.1016/j.jcp.2019.108897>
- [63] Friedrich, L., Winters, A.R., Del Rey Fernández, D.C., Gassner, G.J., Parsani, M., Carpenter, M.H.: An entropy stable h/p non-conforming discontinuous Galerkin method with the summation-by-parts property. *Journal of Scientific Computing* **77**, 689–725 (2018) <https://doi.org/10.1007/s10915-018-0733-7>
- [64] Merriam, M.L.: *An Entropy-based Approach to Nonlinear Stability*. Stanford University, (1989)